

Catalysis uncoupling in a glutamine amidotransferase bienzyme by unblocking the glutaminase active site

**Felix List^{1,2,*}, M. Cristina Vega^{1,3,*}, Adelia Razeto¹, Michaela C. Häger², Reinhard Sterner²
and Matthias Wilmanns^{1,†}**

¹ EMBL Hamburg, Notkestrasse 85, Building 25A, D-22603 Hamburg, Germany.

² University of Regensburg, Institute of Biophysics and Physical Biochemistry, Universitätsstrasse 31,
D-93053 Regensburg, Germany.

³ Present address: Centro de Investigaciones Biológicas (CIB-CSIC), Ramiro de Maeztu 9, 28040
Madrid, Spain.

* These authors contributed equally.

† To whom correspondence should be addressed.

Phone: +49-40-89902-126

Fax: +49-40-89902-149

E-Mail: wilmanns@embl-hamburg.de

Running Title: Catalysis uncoupling in a bifunctional GAT

Summary

Nitrogen is incorporated into various metabolites by multifunctional glutamine amidotransferases *via* reactive ammonia generated by glutaminase hydrolysis of glutamine. Although this process is generally tightly regulated by subsequent synthase activity, little is known about how the glutaminase is inhibited in the absence of an activating signal. Here, we use imidazoleglycerolphosphate synthase as a model to investigate the mechanism of glutaminase regulation. A structure of the bienzyme–glutamine complex reveals that the glutaminase active site is in a catalysis-competent conformation but the ammonia pathway towards the synthase active site is blocked. Mutation of two residues blocking the pathway leads to a complete uncoupling of the two reactions and to a 2800-fold amplification of glutaminase activity. Our data advance the understanding of coupling enzymatic activities in glutamine amidotransferases and raise new hypotheses of the underlying molecular mechanism.

Highlights:

- The ImGP synthase ammonia pathway is blocked in presence of glutaminase substrate
- Two ImGP synthase subunit residues are involved in glutaminase catalysis
- The glutaminase oxyanion hole is properly formed in absence of synthase substrate
- Unblocking the ammonia pathway uncouples the two catalyzed reactions of ImGP

Introduction

Living organisms have a fundamental requirement to make reactive nitrogen available for chemical incorporation into key metabolites by enzyme catalysis. The most widespread category of enzymatic nitrogen donors is represented by multifunctional glutamine amidotransferases (GAT) (Zalkin and Smith, 1998). GATs generate ammonia by glutamine hydrolysis, which is then transported to the synthase active site via a protein tunnel sequestered from the solvent environment (Mouilleron and Golinelli-Pimpaneau, 2007; Raushel et al., 2003). The glutaminase activity of most of these multi-enzymes is coupled with their GAT-specific synthase activity. Whereas the synthase activities are unrelated in known GATs the participating glutaminase domains can be categorized to belong either to the so-called Ntn-type (class II), characterized by an N-terminal catalytic cysteine residues, or to the catalytic dyad type (class I) with a characteristic active site histidine-cysteine arrangement. While conformational changes within the glutaminase/synthase during GAT catalysis have been structurally well characterized for one member of the Ntn-GAT family, glucosamine-6-phosphate synthase (Mouilleron et al., 2011), little has been known about possible conformational changes within the analogous interface of any GAT with a catalytic dyad glutaminase. Because of the structural diversity observed in known GATs, however, it has been difficult to identify a generally applicable mechanism of catalysis coupling, and the molecular details of activity cross-regulation are only poorly understood for most of the enzymes investigated to date.

We chose the heterodimeric imidazoleglycerolphosphate (ImGP) synthase complex from *Thermotoga maritima* as a model system to study the regulation of glutamine hydrolysis within GATases. The synthase subunit (HisF) of this bienzyme complex, also referred to as the cyclase subunit, catalyzes the addition of an amino group to N⁷-[(5'phosphoribulosyl)formimino]-5-

aminoimidazole-4-carboxamide-ribonucleotide (PrFAR), which is subsequently cleaved into 5-aminoimidazole-4-carboxamide ribotide (AICAR) and ImGP (Klem and Davisson, 1993) (**Figure 1, Supplementary Figure S1**). The amino group originates from sequestered ammonia generated by the glutaminase subunit (HisH), which belongs to the family of catalytic **dyad** glutaminases (Zalkin and Smith, 1998). The two products PrFAR and AICAR are further used in the downstream purine and histidine biosynthesis pathways, respectively, thus rendering ImGP synthase a branch-point enzyme in nucleotide and amino acid metabolism. A remarkable property of the *T. maritima* bienzyme is that the glutaminase subunit shows **neither** measurable activity in the absence of the cyclase subunit **nor** in the presence of the cyclase subunit without active site ligands, making the ImGP synthase bienzyme one of the most tightly regulated GATs known to date (Beismann-Driemeyer and Sterner, 2001). By contrast, the separate cyclase subunit of this bienzyme is catalytically active in ammonia-containing solutions at high pH when the $\text{NH}_3/\text{NH}_4^+$ equilibrium is sufficiently shifted towards ammonia.

Several crystal structures of ImGP synthase bienzymes have unraveled how the glutaminase docks onto the N-terminal face of the cyclase $(\beta/\alpha)_8$ -barrel, irrespective of whether the bienzyme is formed by two separate, monofunctional subunits or by a two-domain, bifunctional enzyme (Chaudhuri et al., 2001; Douangamath et al., 2002; Omi et al., 2002). The two active sites are separated by about 25 Å, defining the distance required to transport sequestered ammonia from the glutaminase to the cyclase active site (**Figure 2A**). The glutaminase active site is near the glutaminase/cyclase interface, which contains four invariant, charged residues that provide the framework of the gate to the cyclase ammonia tunnel (**Figure 2B**). The cyclase active site is located at the opposite face of the $(\beta/\alpha)_8$ -barrel and is connected by a tunnel-like structure along the central

barrel axis to the glutaminase/cyclase interface.

To investigate the mechanism of regulated glutamine hydrolysis in ImGP synthase and catalysis coupling with the subsequent synthase reaction (**Figure 1, red bar**), we first determined the molecular parameters of glutaminase substrate binding. A structure of the ImGP synthase bienzyme in complex with glutamine reveals the glutaminase active site to be in a catalysis-competent conformation with a properly formed oxyanion hole. However, in this structure the glutaminase/cyclase interface and the connecting tunnel appear to be blocked. By removing the side chains of two plug-forming residues, we were able to generate up to 2800-fold increased glutaminase activity, which is uncoupled from synthase activity. Our data thus show that coupling of the two catalytic activities in the ImGP synthase bienzyme critically depend on the proper formation of a specific and tight protein/protein interface of the two enzyme units involved in the overall reaction.

Results

The glutaminase active site is in a catalysis-competent conformation

We first carried out a structural analysis of the ImGP synthase bienzyme from *T. maritima* in the presence of the glutaminase substrate glutamine, to gain insight into the atomic glutaminase active site–substrate interactions and to investigate whether substrate binding leads to conformational changes in the glutaminase active site. As the previously reported apo crystal form was unsuitable for these experiments owing to the high salt concentration used for crystallization (Douangamath et al., 2002), we identified a new crystal form with a distinct morphology that grew from polyethylene glycol and glutamine (**Supplementary Table 1**). The structure revealed well-defined density in the glutaminase active site in two of the three ImGP synthase bienzyme complexes that could present either glutamine or glutamate (**Figures 2A and 3A+C**). Since the constitutively active ImGP synthase variant crystallized under the same conditions did not show such density in the glutaminase active site (details below), we interpreted the density to represent the substrate glutamine, confirming that there was no substrate turnover under crystallization conditions in the absence of cyclase ligands as expected from previous biochemical data (Beismann-Driemeyer and Sterner, 2001). The reactive side chain of glutamine is oriented towards the previously identified ammonia-transfer pathway to the cyclase active site (Douangamath et al., 2002).

In the glutaminase active site with bound glutamine, the catalytic dyad residues, Cys84(HisH) and His178(HisH), are found in positions relative to each other and in an orientation towards glutamine that require only minor conformational changes to reach a catalytic Michaelis complex (**Figure 3A+C, Supplementary Figure S2A+C**). The Cys84 sulfhydryl group is within 3.8 Å of the reactive carbon atom of the glutamine side chain and is polarized by the imidazole ring of

His178(HisH). His178(HisH) in turn interacts with Asp98(HisF) from the cyclase subunit via a solvent-mediated hydrogen bond. The non-reactive main-chain end of glutamine forms a hydrogen bond with the side chains of Gln88(HisH) and the invariant Glu96(HisH), and engages in additional interactions with the polar main-chain atoms of Gly52(HisH), Thr142(HisH), and Tyr143(HisH). The reactive amido group of the glutamine side chain is connected by a weak hydrogen bond (3.6 Å) with Gln123(HisF) from the cyclase. Together with the contribution of Asp98(HisF), this observation indicates a direct structural involvement of the cyclase subunit in the glutaminase active site.

In addition, the main-chain amido group of Gly52(HisH) forms a short hydrogen bond with the carbonyl group of the reactive glutamine side chain, allowing its polarization to facilitate glutaminase catalysis (Thoden et al., 1999) (**Figure 3C, Supplementary Figure S2C**).

Gly52(HisH) is part of the conserved PGVG motif (residues 49-52) that provides the oxyanion hole, which is common to many hydrolases and proteases (Ollis et al., 1992; Zalkin and Smith, 1998).

Thus, in the ImGP synthase–glutamine complex, the ‘oxyanion strand’ of the glutaminase subunit is in a catalytically competent conformation (Mouilleron and Golinelli-Pimpaneau, 2007; Myers et al., 2005). A comparison with the apo structure of the same cyclase–glutaminase complex and of the separate glutaminase subunit (Douangamath et al., 2002) revealed no evidence of a potential reorientation of the glutaminase oxyanion hole (**Figure 3, Supplementary Figure S3**).

The glutaminase active site is sequestered from the glutaminase/cyclase interface

The structure of the glutamine-bound glutaminase active site has also allowed a more precise characterization of the ammonia pathway towards the cyclase active site. The glutaminase active

site is sealed off from the glutaminase/cyclase interface. The bulky side chain of Tyr138(HisH) acts like a plug effectively blocking the gate into the ammonia tunnel, which is defined by the cyclase residues Arg5(HisF), Glu46(HisF), Lys99(HisF) and Glu167(HisF) (**Figures 2B and 3A-B**) (Douangamath et al., 2002), from the glutaminase active site. The gate is further blocked by a few neighboring glutaminase residues, including Met121(HisH), Trp123(HisH) and Lys181(HisH). A comparison of the glutamine-bound and the apo structure of the ImGP synthase bienzyme show the presence of the plug, irrespective of whether glutamine is bound to the glutaminase active site (**Supplementary Figure S3**).

These findings suggest that glutamine hydrolysis, which occurs as a consequence of substrate binding to the cyclase active site, could be based on unblocking of the glutaminase active site (**Figure 1, green arrow**). Although the molecular details of the conformational changes required for such mechanism have not yet been determined, our structures indicate that the site of unblocking is centered on the invariant Tyr138(HisH) and neighboring residues from the glutaminase subunit (**Figure 2B**). We subsequently hypothesized that unblocking of the *wt* enzyme could be mimicked by the removal of bulky side chains in these residues, allowing a subsequent functional characterization of the respective enzyme mutants.

Glutaminase activity requires the presence of cyclase residues in the composite glutaminase active site

As a prerequisite for the subsequent experiments, we first tested whether there are residues from the cyclase subunit that are specifically involved in glutaminase activity of the ImGP synthase bienzyme, irrespective of glutaminase activation. To address this question, we selected three

residues from the cyclase subunit that are remote from the cyclase active site: one of them (Lys99) contributes to the ring-shaped gate of the previously postulated ammonia tunnel (Douangamath et al., 2002), and the other two residues Asp98(HisF) and Gln123(HisF) were chosen because of their close proximity to the glutaminase active site (**Figure 3**).

When these residues were individually mutated to alanine, two of the three ImGP synthase complexes, K99A(HisF) and Q123A(HisF), exhibited moderate catalytic efficiency effects in both the cyclase and glutaminase reactions of the bienzyme (**Figure 4A; Table 1**). By contrast, we measured only residual or no glutaminase activity in the D98A(HisF) bienzyme variant, depending on the type of assay used. Moreover, whereas we could detect only slight glutamine-dependent cyclase activity, as expected from the lack of glutaminase activity, the ammonia-dependent cyclase activity of this variant was not affected. These results show that Asp98(HisF) is involved in glutaminase rather than in cyclase activity, thus supporting previous data concerning the analogous mutant of the yeast ImGP synthase bienzyme (Myers et al., 2005). In subsequent work, we used this mutant bienzyme to distinguish the effects on glutaminase activity – originating from the structural requirement to establish a complete functional glutaminase active site irrespective of its state of activation – from effects on other residues directly involved in glutaminase activation (see below).

Unblocking of the glutaminase active site generates constitutive glutaminase activity

To investigate any glutaminase activity-inducing effects from ligand binding to the cyclase active site, we used the closely related substrate analogue N⁷-((5'phosphoribosyl)formimino)-5-aminoimidazole-4-carboxamide-ribonucleotide (PrFAR) because of its higher stability rather than the more labile cyclase substrate PrFAR (Beismann-Driemeyer and Sterner, 2001). In all

experiments we measured substrate turnover (k_{cat}) and where possible substrate binding (K_M) as well, allowing to determine catalytic efficiencies (k_{cat}/K_M). For further details, see the Methods section and **Table 1**.

To test the functional role of the glutaminase active-site plug observed in the structure of the ImGP synthase bienzyme (**Figure 2**), we mutated two glutaminase residues from the plug, Tyr138(HisH) and Lys181(HisH), into alanines. In these variants the glutaminase catalytic efficiency in the presence of the cyclase ligand ProFAR was increased 77-fold and 50-fold, respectively, when compared to *wt* ImGP synthase (**Figure 4A; Table 1**). Moreover, the glutaminase turnover rates of these mutants were increased 45-fold and 86-fold in the absence of ProFAR, thus generating a bienzyme system with significant constitutive glutaminase activity. [The observed effect of the exchange K181A\(HisH\) is in agreement with a previous finding on the type of mutation in the corresponding lysine in the yeast ImGP synthase bienzyme \(Myers et al., 2005\).](#) In the double mutant [Y138A(HisH), K181A(HisH)], constitutive substrate turnover in the absence of ProFAR was further amplified, resulting in glutaminase turnover that was 2800-fold higher than that of the *wt* ImGP synthase bienzyme. The catalytic efficiency of this mutant in the presence of ProFAR was 115-fold increased over that observed for the *wt* enzyme. The glutamine turnover numbers of this double mutant in the presence or absence of ProFAR were quite similar at 2.4 s^{-1} and 1.4 s^{-1} , respectively, indicating that any activity-inducing effect by ProFAR is negligible. Remarkably, these turnover numbers are more than tenfold higher than the k_{cat} -value of the *wt* enzyme in the presence of ProFAR.

Neither the glutamine- nor the ammonia-dependent cyclase activities of the ImGP synthase variants are compromised significantly (**Table 1**), indicating that the mutations do not affect the integrity of

the cyclase active site. Since the absolute synthase turnover numbers are, however, lower than that of the glutaminase it is likely that some of the ammonia produced by the glutaminase subunit leaks from the ammonia transfer path in those ImGP synthase mutants with synthase-independent constitutive glutaminase activity.

Our data demonstrate that the removal of the bulky side chains of the residues that plug the glutaminase active site – Tyr138(HisH) and Lys181(HisH) – abolishes the requirement for cyclase substrate binding to stimulate glutaminase activity in the ImGP synthase complex (**Figure 1, green arrow**) and unleashes the intrinsic glutaminase activity in the ImGP synthase bienzyme. By contrast, the separate glutaminase subunit Y138A(HisH) and K181A(HisH) variants remained inactive (data not shown), confirming that glutaminase/cyclase complex formation is a prerequisite for glutaminase activity of the ImGP synthase bienzyme. However, when combining the exchanges Y138A(HisH) and D98A(HisF), the resulting ImGP synthase variant showed only residual glutaminase activity in the presence of ProFAR (< 1%) and strongly reduced activity in its absence (3%), using the glutaminase activity of Y138A(HisH) as a reference (**Table 1**). These data confirm that Asp98(HisF) is involved in glutaminase catalysis, independent of the requirement for cyclase catalysis.

The constitutive glutaminase activity of ImGP variants containing Y138A(HisH), K181A(HisH), and [Y138A(HisH), K181A(HisH)] was confirmed by following ammonia production. This was achieved by measuring the glutamate dehydrogenase-catalyzed NADH/H⁺ oxidation to NAD⁺ (**Figure 4B, Supplementary Figure S4D**), rather than the opposite process that was used to measure glutamate production (**Figure 4A, Supplementary Figure S4C**). In the presence of saturating concentrations of ProFAR and glutamine, the glutaminase variants Y138A(HisH) and

K181A(HisH) generate ammonia at rates of 2.2 s^{-1} and 3.3 s^{-1} , which are similar to their rates for glutamate production (3.0 s^{-1} and 2.4 s^{-1} ; **Table 1**). Similarly, the turnover numbers of the double mutant [Y138A(HisH), K181A(HisH)] in the presence of ProFAR as measured by following glutamate production (2.4 s^{-1}) and ammonia production (1.9 s^{-1}) are in good agreement. For comparison, in the *wt* ImGP synthase bienzyme, the measured rate of ammonia production was 0.04 s^{-1} , which is also similar to the detected rate of glutamate formation under the same conditions (0.10 s^{-1}) (**Table 1**).

The structure of the ImGP synthase [Y138A(HisH), K181A(HisH)] variant confirms unblocking of the glutaminase active site

We further validated our biochemical findings by solving the crystal structure of the ImGP synthase [Y138A(HisH), K181A(HisH)] double mutant (**Supplementary Table 1; Figure 3B+D**). The structure indeed revealed that, in contrast to *wt* ImGP synthase, the glutaminase active site was empty, despite glutamine being present in the crystallization medium for both enzymes. This observation is in agreement with constitutive glutamine turnover and product release by the [Y138A(HisH), K181A(HisH)] mutant ImGP synthase complex. Similar to the other ImGP synthase bienzyme structures, the overall conformation of the glutaminase active site remains unchanged, indicating a catalysis-competent conformation that includes a properly formed oxyanion hole.

However, a comparative analysis with the structures of the *wt* bienzyme reveals that the approximately 1100 \AA^2 heterodimeric glutaminase/cyclase interface of the *wt* bienzyme is reduced by at least 150 \AA^2 in the [Y138A(HisH), K181A(HisH)] double mutant, which corresponds to about

15% of the overall interface. In the mutant structure a large cavity is generated with eight ordered solvent molecules occupying the space normally required for the bulky side chains of Tyr138(HisH) and Lys181(HisH) in the *wt* bienzyme (**Figure 3B**). The structure confirms that unplugging of the glutaminase active site increases the solvent exposure of the glutaminase active site and opens the entrance to the ammonia channel leading to the cyclase active site (**Figure 5**).

Discussion

Here, we have shown that a GAT bienzyme system with constitutive and amplified glutaminase activity can be generated with an ImGP synthase bienzyme variant, in which the path between the glutaminase active site, the glutaminase/cyclase interface and the cyclase ammonia tunnel is opened, thus effectively uncoupling glutaminase and cyclase catalysis. The 2800-fold increase in unregulated glutaminase turnover, observed in the [Y138A(HisH), K181A(HisH)] ImGP synthase mutant, is without precedence in known GATs. Here, we discuss our findings in the light of previously proposed glutaminase activation mechanisms.

A common feature of ImGP synthases from different organisms is that their glutaminase activity can be induced by the cyclase substrate PrFAR, by the substrate analogue ProFAR and by the product ImGP (Beismann-Driemeyer and Sterner, 2001; Myers et al., 2005; Myers et al., 2003) (**Figure 1, green arrow**). The homologous ImGP synthase from yeast has biochemical and structural properties related to the heterodimeric complex from *T. maritima* (Chaudhuri et al., 2003; Myers et al., 2005; Myers et al., 2003). However, in contrast to the latter enzyme, it comprises both catalytic activities on the same polypeptide chain. Recent biochemical and molecular dynamics data from the yeast ImGP synthase favored an allosteric activation of glutamine hydrolysis (Amaro et al.,

2003; Myers et al., 2005). Based on these findings a signaling mechanism was proposed, originating from ligand binding to the cyclase active site and then transmitted to the glutaminase active site *via* several residue segments along the ammonia-transfer pathway of ImGP synthase. In this model, a conformational change of the oxyanion hole in the glutaminase active site was considered to be the terminal step that induces glutaminase catalysis (Chaudhuri et al., 2003; Myers et al., 2005).

However, our structural data from the ImGP synthase–glutamine complex, a previous apo structure of the same bienzyme and another structure of the separate glutaminase subunit (Douangamath et al., 2002) have consistently revealed a catalytically competent conformation of the oxyanion hole (**Figure 3C, Supplementary Figure S3**). We therefore re-examined all available ImGP synthase structures with respect to the observed glutaminase active-site conformation. A comparison reveals that the interaction that was thought to be crucial for oxyanion formation (Gly50) in the yeast ImGP synthase structure (Chaudhuri et al., 2003) is out of register by one residue with respect to our observations in the *T. maritima* ImGP synthase–glutamine complex structure (**Figure 6A-B**). The structure of the *T. maritima* ImGP synthase bienzyme shows that the next residue (Gly51) is in an active conformation and interacts *via* its main-chain amido group with the carbonyl side-chain group of bound glutamine (**Figure 3C, Supplementary Figure S2C**), thus polarizing the reactive amido group and increasing its susceptibility for hydrolysis. Most likely, the lack of a functional oxyanion hole identified in the previous structure of the yeast bienzyme was because it was determined in the presence of the glutaminase inhibitor acivicin (Chaudhuri et al., 2003) rather than the native glutaminase substrate glutamine. Our structure of the ImGP synthase–glutamine complex also does not confirm a previously postulated reorientation of glutamine upon glutaminase activation (Myers et al., 2005), as glutamine is in an orientation expected to be competent for the

release of ammonia into the glutaminase/cyclase-connecting tunnel.

Our finding of a mostly rigid and catalysis-competent active-site conformation with a properly formed oxyanion hole in the glutaminase subunit is, however, in agreement with the structures of at least three other glutaminase-glutamine substrate complexes, including those of carbamoyl phosphate synthetase (Thoden et al., 1999), pyridoxal 5'-phosphate synthase (Strohmeier et al., 2006), and cytidine triphosphate synthetase (Goto et al., 2004). We illustrate this by a comparison with the carbamoyl phosphate synthetase–glutamine complex structure (**Figure 6C-D**). In the catalytic dyad glutaminase domain of this enzyme, the function of Gly241 is identical to that of Gly52 in the ImGP synthase complex, namely to activate the reactive side-chain group of glutamine (Thoden et al., 1999). In reference to these comparisons, we argue that cyclase substrate-induced glutaminase activation most likely occurs through unblocking of the glutaminase active site (**Figure 5**) rather than leading to activating conformational changes of essential glutaminase active site residues.

We finally wondered how unblocking of the ammonia gateway in glutaminase/synthase interface could lead to the activation of synthase-independent glutaminase activity. Probably the most detailed analysis of a catalytic dyad type glutamine amidotransferase, to date, has been carried out in carbamoyl phosphate synthetase (Thoden et al., 1998). Assuming that the mechanistic findings apply to the ImGP synthase bienzyme as well, in principle, any glutaminase catalysis step – active site cysteine-mediated attack of glutamine, thioester intermediate formation, and thioester hydrolysis – could be affected by glutaminase active site unplugging. Characterization of a separate glutaminase mutant with constitutive activity from another GAT – anthranilate synthase – showed that a single amino acid exchange close to the active site leads to the activation of the catalytic

cysteine. As a consequence, the formation of the thioester, which was shown to be rate-limiting for the overall glutaminase reaction, was substantially accelerated (List et al., 2012).

Although we cannot exclude that the activating effect of the Y138A and K181A exchanges is based on a similar mechanism, the crystal structure of the [Y138A(HisH), K181A(HisH)] ImGP synthase mutant suggests alternate activation mechanisms. One option could be that unblocking of the glutaminase active site facilitates access of bulk water to the glutaminase active site, thus promoting hydrolysis of the thioester intermediate. [A second option could be an improved positioning of Asp98 \(HisF\) to participate in the glutaminase active site, due to removal of the side chains of Tyr138 \(HisH\) and Lys181 \(HisH\). As Lys181 \(HisH\) is involved into a salt bridge with Asp98 \(HisF\), one could speculate that removal of this interaction specifically leads to increased conformational flexibility of Asp98 \(HisF\). However, the effect of mutating Lys181 is actually weaker than that of mutating Tyr138 \(HisH\). Alternatively, presenting a third option, the opening of the channel gate might allow for a more efficient transport of ammonia to the cyclase active site. Such mechanism, favored by our observations, would be in agreement with early studies, postulating that ammonia sequestration in GATs would lead to product inhibition of glutaminase activity in the absence of synthase activity \(Messenger and Zalkin, 1979; Milman et al., 1980; Raushel et al., 1978\), supporting classical and well-established mechanisms of catalysis regulation by product inhibition \(Frieden and Walter, 1963; Rudolph, 1979\).](#)

Whereas there is no doubt about the effect of cyclase substrate binding (or related compounds) to induce coupled glutaminase/cyclase catalysis, questions remain on the role of specific cyclase residues that are remote from the cyclase active site in this allosteric activation mechanism. Molecular dynamic simulations and recent nuclear magnetic resonance (NMR) data indicate that

this signaling mechanism could be a rather delocalized process with slow time scales (Amaro et al., 2007; Liebold et al.; Lipchock and Loria; Rivalta et al., 2012). However, plugging/unplugging of the cyclase ammonia tunnel gate, comparable to our findings, has not been discussed in these contributions.

In addition, it remains unknown whether the gate to the cyclase ammonia tunnel (**Figure 2B**) forms a bottleneck in the transfer of ammonia from the glutaminase to the cyclase active site (Amaro et al., 2003; Douangamath et al., 2002; Myers et al., 2003) and whether conformational changes of these tunnel residues can be induced by glutaminase residues such as Tyr138(HisH), as proposed previously (Chaudhuri et al., 2001). This is in agreement with available biochemical data from various cyclase variants of the *T. maritima* and yeast ImGP synthase, none of which indicated increased and/or uncoupled glutaminase activity (Amaro et al., 2005; Beismann-Driemeyer and Sterner, 2001; Myers et al., 2005; Myers et al., 2003). However, the close structural proximity of several ammonia gate residues to the cyclase subunit (**Figure 2B**) suggests that they may play a role in triggering conformational changes of Tyr138(HisH) to unplug the glutaminase active site, as part of the previously suggested allosteric mechanism of glutaminase activation by cyclase substrate binding. This hypothesis, however, still needs further to be experimentally validated.

In conclusion, our new findings, together with previous data from several other laboratories, show that despite the general purpose of ammonia transfer each GATase system differs substantially in terms of specific mechanism for glutaminase regulation and ammonia transfer (Goto et al., 2004; Guedez et al., 2012; Strohmeier et al., 2006). Taking our data together, a mechanism emerges for ImGP in which glutaminase activity is induced by the unplugging of its active site (**Figures 1 and 5**). A complete understanding of the underlying molecular mechanism of ImGP synthase activity

coupling, and possibly those of related GATs, will require a precise tracing of the glutaminase products, ammonia and glutamate, during the bienzyme catalysis steps subsequent to glutaminase hydrolysis. Understanding and having control over these parameters could ultimately allow engineering of GATs with optimized glutaminase activities that enable incorporation of nitrogen into novel heterocyclic compounds.

Significance

Living organisms have a fundamental requirement to generate reactive nitrogen for incorporation into various metabolites. The family of multifunctional glutamine amidotransferases presents the most widespread category of *in situ* nitrogen donors. These enzymes generate reactive ammonia by glutamine hydrolysis, followed by ammonia transport *via* a sequestered tunnel and consumption by enzyme-specific synthase activities. To avoid wasteful loss of glutamine, its hydrolysis by the glutaminase needs to be tightly linked with the synthase reaction. However, the molecular mechanism of glutaminase/synthase catalysis coupling has remained enigmatic. We chose the imidazoleglycerolphosphate synthase as a model to investigate how glutaminase activity could be induced in the context of such multifunctional enzyme by a combined biochemical and structural biology approach. Contrary to several hypotheses in the field, we found that the active site of the glutaminase subunit is in a catalysis-competent conformation in all conformational states we captured structurally but bound substrate glutamine is not hydrolyzed to glutamate and ammonia. Remarkably, when removing the bulky side chains of two key residues in the glutaminase/synthase interface, we observed a complete decoupling of the two catalytic activities and an increase of constitutive glutamine turnover by more than three orders of magnitude. Our findings provide novel insights into catalysis coupling in glutamine amidotransferases specifically and multifunctional

enzymes in general. Our tools to control the amount of ammonia production in imidazoleglycerolphosphate synthase could be applicable on the efficient synthesis of other nitrogen-containing compounds, and thus may lead to important new applications in biotechnology and chemistry.

Experimental Procedures

Materials. All chemicals, buffers, enzymes and resins were purchased from commercial sources. The synthesis of ProFAR was performed as previously described (Davisson et al., 1994).

DNA manipulation and sequence analysis. Preparation of DNA, digestion with restriction endonucleases, and DNA ligation were performed as described (Beismann-Driemeyer and Sterner, 2001). Oligonucleotides were purchased from Metabion. DNA was amplified by PCR using *Taq* or *Pwo* polymerase (Roche Diagnostics, Fermentas), extracted from agarose gels using the QIAquick gel extraction kit (Qiagen), and commercially sequenced (Geneart) with standard methods.

Site-directed mutagenesis and subcloning. The *hisF* mutant genes D98A, K99A, Q123A and the *hisH* mutant gene Y138A were produced by overlap extension PCR (Ho et al., 1989; Horton et al., 1989) using the plasmids pET11c-*hisF* (Thoma et al., 1999) and pDS56/RBSII-*hisH* (Beismann-Driemeyer and Sterner, 2001), respectively, as templates. The *hisF*-D98A and *hisF*-Q123A genes were cloned into pET11c (Novagen), *hisF*-K99A was cloned into pET24a (Novagen), and *hisH*-Y138A was cloned into pDS/RBSII (Stüber et al., 1981). To confirm the introduced base substitutions and to exclude inadvertent point mutations, all mutated genes were fully sequenced. The *hisA* gene, encoding N'-((5'phosphoribosyl)formimino)-5-aminoimidazole-4-carboxamide-ribonucleotide (ProFAR) isomerase from *T. maritima*, was amplified by PCR using pDS56/RBSII-

hisA (Thoma et al., 1999) as template and sub-cloned into pET21a (Novagen) using newly introduced *NdeI* and *NotI* restriction sites. The expression of the *hisA* gene from pET21a resulted in the addition of a C-terminal His₆ tag to the recombinant protein product.

Heterologous gene expression and protein purification. The HisF variants were produced by heterologous gene expression in *Escherichia coli* strain BL21(DE3) (Stratagene). The HisH variants were produced in *E. coli* strain W3110 Δ *trpEA2* (Schneider et al., 1981) containing the helper plasmid pDMI,1 as described for HisA from *T. maritima* (Thoma et al., 1999). The recombinant protein products were purified from the soluble fraction of the crude extract by heat precipitation of the host proteins (20 min at 70 °C), followed by ion exchange chromatography. To this end, the supernatant of the heat step was loaded onto a MonoQ column (HR 16/10, 20 ml, Pharmacia), which had been equilibrated with 50 mM potassium phosphate (pH 7.5). The column was washed with the equilibration buffer, and bound protein was eluted by applying a linear gradient of 0 – 1.5 M NaCl. Fractions with pure protein were pooled and dialyzed extensively against 50 mM potassium phosphate (pH 7.5). The HisF-K99A, HisH and HisH-Y138A proteins were additionally subjected to ammonia sulfate precipitation. [To remove the ammonium sulphate from the precipitated protein, the ammonium sulphate pellet was resuspended in 50 mM potassium phosphate \(pH 7.5\) and extensively dialysed twice against the same buffer.](#) HisA from *T. maritima* was also produced by heterologous gene expression in *E. coli* BL21(DE3) (Stratagene). The recombinant protein was purified from the soluble fraction of the crude extract by heat precipitation (15 min at 73 °C) of the host proteins, followed by metal chelate affinity chromatography. To this end, the extract was loaded onto a nickel Sepharose column (HisTrap FF crude 5 ml; GE Healthcare) that had been equilibrated with 50 mM potassium phosphate, 300 mM NaCl, 1 mM imidazole (pH 7.5).

The column was washed with the equilibration buffer, and the bound His₆-tagged protein was eluted by applying a linear gradient of 1-300 mM imidazole. Fractions with pure protein were pooled and dialyzed extensively against 50 mM potassium phosphate (pH 7.5). Based on SDS-PAGE analysis, the purity of all samples was at least 90%. Yields were 2–6 mg of protein per gram of wet cell mass. The proteins were dripped into liquid nitrogen and stored at -80 °C.

Steady-state kinetics. The glutamine- and ammonia-dependent cyclase activities of the ImGP synthase bienzyme (**Supplementary Figure S4A-B**) were measured at 25 °C as previously described, using PrFAR produced *in situ* from ProFAR by HisA from *T. maritima* as the substrate (Beismann-Driemeyer and Sterner, 2001; Klem and Davisson, 1993). The values for K_m^{PrFAR} and V_{max} were deduced from initial velocity measurements performed in the presence of various concentrations of PrFAR. The glutaminase activity of ImGP synthase in the presence of stimulating ProFAR was measured at 25 °C, by following either glutamate (**Supplementary Figure S4C**) (Beismann-Driemeyer and Sterner, 2001), or ammonia production (**Supplementary Figure S4D**), in a coupled enzymatic assay with glutamate dehydrogenase (GDH) as the helper enzyme, and either NAD⁺ or NADH as the coenzyme. The values for K_m^{Gln} and V_{max} were deduced from initial velocity measurements performed in the presence of various concentrations of L-glutamine. In order to circumvent the stimulating effect of NAD⁺ on glutaminase activity, glutamate production in the absence of ProFAR was measured at 25 °C in a discontinuous assay, in the presence of saturating glutamine concentrations. To this end, 150 µl aliquots of the reaction mixture were collected after 20, 40 and 60 min (3, 8, 13 min in the case of [Y138A(HisH), K181A(HisH)]), and spun through a 10 kDa filter to remove ImGP synthase. V_{max} was calculated from the linear increase of produced glutamate with time, which was determined with the help of GDH and NAD⁺. The precise reaction

conditions are provided in the **Supplementary Information**.

Crystallization: All crystallization experiments were carried out by the sitting-drop vapor-diffusion method at 20 °C, using drops consisting of protein at a concentration of 23-38 mg/ml in a buffer containing 10 mM Tris-HCl, pH 7.5, 10 mM dithiotreitol (DTT), and 2 µl reservoir solution (100 mM Hepes, pH 8.5, 15%-19% (w/v) polyethylene glycol 8000, 45 mM ammonium nitrate/acetate, 5% (v/v) methyl-2,4-pentane-diol, 10 mM DTT), supplemented with 20 mM L-glutamine. Suitable crystals of the [Y138A(HisH), K181A(HisH)] ImGP synthase variant were obtained by micro-seeding pre-equilibrated crystallization drops, containing 12 mg/ml protein and 11% [v/w] polyethylene glycol 8000. All crystals were cryo-protected in 20% (v/v) glycerol. Details of X-ray structure determination are described in the **Supplementary Information**.

Structure analysis: The structural superpositions of ImGP synthase complexes were carried out with SSM (Krissinel and Henrick, 2004). The interface areas (complementary colors) were determined with the program AREAIMOL from the CCP4 suite (1994; Lee and Richards, 1971).

All structural graphics, including the tunnel presentations, have been prepared with the Pymol software (<http://pymol.org/>).

PDB codes: Atomic coordinates and structure factor amplitudes for the four complexes described here have been deposited in the Protein Data Bank (PDB) with the following codes: 3ZR4 (glutamine complex); 2WJZ ([Y138A(HisH), K181A(HisH)] ImGP synthase variant).

Acknowledgments: This work was supported by grants from the Deutsche Forschungsgemeinschaft to R.S. (STE 891/3-3, 3-4) and M.W. (WI 1058/5-3, 5-4). We thank Jochen Kuper (University of Würzburg, Germany) and Karin Babinger (University of Regensburg,

Germany) for technical assistance during the project, and Maja Koehn (EMBL, Heidelberg, Germany) for critical comments. M.W. and R.S coordinated the project and designed the experiments. The biochemical experiments were carried out by F.L. and M.C.H. X-ray structural analysis was carried out by M.C.V and A.R. M.W. compiled the manuscript.

References:

- Amaro, R., Tajkhorshid, E., and Luthey-Schulten, Z. (2003). Developing an energy landscape for the novel function of a (beta/alpha)₈ barrel: ammonia conduction through HisF. *Proc Natl Acad Sci U S A* 100, 7599-7604.
- Amaro, R.E., Myers, R.S., Davisson, V.J., and Luthey-Schulten, Z.A. (2005). Structural elements in IGP synthase exclude water to optimize ammonia transfer. *Biophys J* 89, 475-487.
- Amaro, R.E., Sethi, A., Myers, R.S., Davisson, V.J., and Luthey-Schulten, Z.A. (2007). A network of conserved interactions regulates the allosteric signal in a glutamine amidotransferase. *Biochemistry* 46, 2156-2173.
- Beismann-Driemeyer, S., and Sterner, R. (2001). Imidazole glycerol phosphate synthase from *Thermotoga maritima*. Quaternary structure, steady-state kinetics, and reaction mechanism of the hienzyme complex. *J Biol Chem* 276, 20387-20396.
- CCP4 (1994). The CCP4 suite: programs for protein crystallography. *Acta Crystallogr D Biol Crystallogr* 50, 760-763.
- Chaudhuri, B.N., Lange, S.C., Myers, R.S., Chittur, S.V., Davisson, V.J., and Smith, J.L. (2001). Crystal Structure of Imidazole Glycerol Phosphate Synthase. A Tunnel through a (beta/alpha)₈ Barrel Joins Two Active Sites. *Structure (Camb)* 9, 987-997.
- Chaudhuri, B.N., Lange, S.C., Myers, R.S., Davisson, V.J., and Smith, J.L. (2003). Toward understanding the mechanism of the complex cyclization reaction catalyzed by imidazole

glycerolphosphate synthase: crystal structures of a ternary complex and the free enzyme.

Biochemistry 42, 7003-7012.

Davisson, V.J., Deras, I.L., Hamilton, S.E., and Moore, L.L. (1994). A plasmid-based approach for the synthesis of a histidine biosynthetic intermediate. *J. Org. Chem.* 58, 137 – 143.

Douangamath, A., Walker, M., Beismann-Driemeyer, S., Vega-Fernandez, M.C., Sterner, R., and Wilmanns, M. (2002). Structural evidence for ammonia tunneling across the (beta alpha)₈ barrel of the imidazole glycerol phosphate synthase hienzyme complex. *Structure* 10, 185-193.

Frieden, E., and Walter, C. (1963). Prevalence and significance of the product inhibition of enzymes. *Nature* 198, 834-837.

Goto, M., Omi, R., Nakagawa, N., Miyahara, I., and Hirotsu, K. (2004). Crystal structures of CTP synthetase reveal ATP, UTP, and glutamine binding sites. *Structure* 12, 1413-1423.

Guedez, G., Hipp, K., Windeisen, V., Derrer, B., Gengenbacher, M., Bottcher, B., Sinning, I., Kappes, B., and Tews, I. (2012). Assembly of the eukaryotic PLP-synthase complex from *Plasmodium* and activation of the Pdx1 enzyme. *Structure* 20, 172-184.

Ho, S.N., Hunt, H.D., Horton, R.M., Pullen, J.K., and Pease, L.R. (1989). Site-directed mutagenesis by overlap extension using the polymerase chain reaction. *Gene* 77, 51-59.

Horton, R.M., Hunt, H.D., Ho, S.N., Pullen, J.K., and Pease, L.R. (1989). Engineering hybrid genes without the use of restriction enzymes: gene splicing by overlap extension. *Gene* 77, 61-68.

Klem, T.J., and Davisson, V.J. (1993). Imidazole glycerol phosphate synthase: the glutamine

amidotransferase in histidine biosynthesis. *Biochemistry* 32, 5177-5186.

Krissinel, E., and Henrick, K. (2004). Secondary-structure matching (SSM), a new tool for fast protein structure alignment in three dimensions. *Acta Crystallogr D Biol Crystallogr* 60, 2256-2268.

Lee, B., and Richards, F.M. (1971). The interpretation of protein structures: estimation of static accessibility. *J Mol Biol* 55, 379-400.

Liebold, C., List, F., Kalbitzer, H.R., Sterner, R., and Brunner, E. (2010). The interaction of ammonia and xenon with the imidazole glycerol phosphate synthase from *Thermotoga maritima* as detected by NMR spectroscopy. *Protein Sci* 19, 1774-1782.

Lipchock, J.M., and Loria, J.P. (2010). Nanometer propagation of millisecond motions in V-type allostery. *Structure* 18, 1596-1607.

List, F., Bocola, M., Haeger, M.C., and Sterner, R. (2012). Constitutively active glutaminase variants provide insights into the activation mechanism of anthranilate synthase. *Biochemistry* 51, 2812-2818.

Messenger, L.J., and Zalkin, H. (1979). Glutamine phosphoribosylpyrophosphate amidotransferase from *Escherichia coli*. Purification and properties. *J Biol Chem* 254, 3382-3392.

Milman, H.A., Cooney, D.A., and Huang, C.Y. (1980). Studies on the mechanism of the glutamine-dependent reaction catalyzed by asparagine synthetase from mouse pancreas. *J Biol Chem* 255, 1862-1866.

- Mouilleron, S., Badet-Denisot, M.A., Badet, B., and Golinelli-Pimpaneau, B. (2011). Dynamics of glucosamine-6-phosphate synthase catalysis. *Arch Biochem Biophys* 505, 1-12.
- Mouilleron, S., and Golinelli-Pimpaneau, B. (2007). Conformational changes in ammonia-channeling glutamine amidotransferases. *Curr Opin Struct Biol* 17, 653-664.
- Myers, R.S., Amaro, R.E., Luthey-Schulten, Z.A., and Davisson, V.J. (2005). Reaction coupling through interdomain contacts in imidazole glycerol phosphate synthase. *Biochemistry* 44, 11974-11985.
- Myers, R.S., Jensen, J.R., Deras, I.L., Smith, J.L., and Davisson, V.J. (2003). Substrate-induced changes in the ammonia channel for imidazole glycerol phosphate synthase. *Biochemistry* 42, 7013-7022.
- Ollis, D.L., Cheah, E., Cygler, M., Dijkstra, B., Frolow, F., Franken, S.M., Harel, M., Remington, S.J., Silman, I., Schrag, J., and et al. (1992). The alpha/beta hydrolase fold. *Protein Eng* 5, 197-211.
- Omi, R., Mizuguchi, H., Goto, M., Miyahara, I., Hayashi, H., Kagamiyama, H., and Hirotsu, K. (2002). Structure of imidazole glycerol phosphate synthase from *Thermus thermophilus* HB8: open-closed conformational change and ammonia tunneling. *J Biochem (Tokyo)* 132, 759-765.
- Raushel, F.M., Anderson, P.M., and Villafranca, J.J. (1978). Kinetic mechanism of *Escherichia coli* carbamoyl-phosphate synthetase. *Biochemistry* 17, 5587-5591.
- Raushel, F.M., Thoden, J.B., and Holden, H.M. (2003). Enzymes with molecular tunnels. *Acc*

Chem Res 36, 539-548.

Rivalta, I., Sultan, M.M., Lee, N.S., Manley, G.A., Loria, J.P., and Batista, V.S. (2012). Allosteric pathways in imidazole glycerol phosphate synthase. *Proc Natl Acad Sci U S A* 109, E1428-1436.

Rudolph, F.B. (1979). Product inhibition and abortive complex formation. *Methods Enzymol* 63, 411-436.

Schneider, W.P., Nichols, B.P., and Yanofsky, C. (1981). Procedure for production of hybrid genes and proteins and its use in assessing significance of amino acid differences in homologous tryptophan synthetase alpha polypeptides. *Proc Natl Acad Sci U S A* 78, 2169-2173.

Strohmeier, M., Raschle, T., Mazurkiewicz, J., Rippe, K., Sinning, I., Fitzpatrick, T.B., and Tews, I. (2006). Structure of a bacterial pyridoxal 5'-phosphate synthase complex. *Proc Natl Acad Sci U S A* 103, 19284-19289.

Stüber, D., Matile, H., and Garotta, G. (1981). Vol 4 (Orlando, FL: Academic Press).

Thoden, J.B., Huang, X., Raushel, F.M., and Holden, H.M. (1999). The small subunit of carbamoyl phosphate synthetase: snapshots along the reaction pathway. *Biochemistry* 38, 16158-16166.

Thoden, J.B., Miran, S.G., Phillips, J.C., Howard, A.J., Raushel, F.M., and Holden, H.M. (1998). Carbamoyl phosphate synthetase: caught in the act of glutamine hydrolysis. *Biochemistry* 37, 8825-8831.

Thoma, R., Obmolova, G., Lang, D.A., Schwander, M., Jenö, P., Sterner, R., and Wilmanns, M.

(1999). Efficient expression, purification and crystallisation of two hyperthermostable enzymes of histidine biosynthesis. FEBS Lett 454, 1-6.

Zalkin, H., and Smith, J.L. (1998). Enzymes utilizing glutamine as an amide donor. Adv Enzymol Relat Areas Mol Biol 72, 87-144.

Figure Legends

Figure 1: Scheme outlining the processes involved in the ImGP synthase bienzyme. Our data suggest that the ImGP synthase bienzyme is regulated by glutaminase residues, indicated in red as “ammonia plug”, that seal the glutaminase active site from the ammonia-transfer pathway to the cyclase active site (red bar) in the absence of an activity-inducing signal from the cyclase active site (green arrow). Generation of AICAR (a,b, *cf.* **Supplementary Figure S4A-B**), glutamate (Glu; c, *cf.* **Supplementary Figure S4C**) and ammonia (NH₃; d, *cf.* **Supplementary Figure S4D**) were measured by different steady-state assays (**Table 1**). The lower part of the scheme indicates how the processes match the overall topography of the heterodimeric glutaminase/cyclase structure (*cf.* **Figure 2**).

Figure 2: Ammonia pathway in the ImGP synthase bienzyme from *T. maritima*. (A) Relevant parts of the cyclase (HisF) and glutaminase (HisH) surfaces, including the active sites, the glutaminase/cyclase interface, and the cyclase ammonia tunnel, are shown in orange (cyclase) and cyan (glutaminase). The ribbons of the structures of these subunits are shown in corresponding lighter colors. The glutamine bound to the glutaminase active site (*cf.* **Figure 3**) is shown by solid spheres with atom-specific colors. The dimensions of the overall structure are indicated to the left. (B) Zoom in to the glutaminase active-site plug, established by Tyr138(HisH), Met121(HisH) and several other residues (not shown for reasons of clarity). This plug seals the remaining part of the ammonia path from the glutaminase active site towards the cyclase active site. The four cyclase residues (Arg5, Glu46, Lys99, Glu167) that establish the gate into the tunnel are also shown.

Figure 3: Glutaminase active site and active-site plug in the ImGP synthase bienzyme. (A) and (C) *wt* bienzyme; (B) and (D) [Y138A(HisH), K181A(HisH)] double mutant. Several residues are highlighted by stick representation of their side chains and are labeled. Color codes are as in **Figure 2**. Ordered solvent molecules are displayed by solid spheres. Hydrogen bonds of less than 3.6 Å distance are shown by dashed lines. The glutaminase approximate location of the glutaminase active site plug is indicated by boxes in panels A, and B. Mutated residues are labeled in red in panel B. The final electron density of bound glutamine is shown at 1.5σ in panel C. [A stereo version of this figure is shown in the supplement \(Supplementary Figure S2\).](#)

Figure 4: Glutaminase and cyclase activities of ImGP synthase variants. (A) Relative catalytic efficiencies at a logarithmic scale using the rates of the *wt* ImGP synthase bienzyme as a reference ($\ln(k_{cat}/K_M) = 0$). Values > 0 indicate gain-of-function, values < 0 indicate loss-of-function. Cyan bars, glutaminase activity as monitored by glutamate production (**Supplementary Figure S4C**), in the presence of saturating concentrations of ProFAR; orange bars, glutamine-dependent cyclase activity (**Supplementary Figure S4A**). The complete set of kinetic data is listed in **Table 1**. (B) Glutaminase activity as monitored by ammonia production (**Supplementary Figure S4D**), in the presence of saturating concentrations of ProFAR and glutamine. Representative curves are shown over a time-interval of 10 minutes for *wt* ImGP synthase, K181A(HisH), Y138A(HisH) and [Y138A, K181A(HisH)].

Figure 5: Sequestration of the glutaminase active site from the ammonia pathway to the cyclase active site in the ImGP synthase enzyme. (A) Although the substrate glutamine can be bound to the glutaminase active site (*cf.* **Figure 3C**), there is no measurable glutaminase activity in *wt* ImGP synthase (HisH active site in red); (B) Unplugging of the glutaminase active site in the

ImGP synthase [Y138A(HisH), K181A(HisH)] double mutant generates a bienzyme with uncoupled and amplified glutaminase activity (HisH active site, green); (C) Cyclase substrate binding (PrFAR, or related ligands, see text for details) to the cyclase active site (HisF active site in green) induces glutaminase activity (HisH active site in green) by a mechanism that is probably also based on glutaminase active site unplugging.

Figure 6: Comparison of the glutaminase active sites of ImGP synthase from *Saccharomyces cerevisiae*, ImGP synthase from *Thermotoga maritima*, and carbamoyl phosphate synthetase (CPS) from *Escherichia coli*. The active site structures of the glutamine complexes of ImGP synthase from *T. maritima* (this contribution) and of carbamoyl phosphate synthetase (CPS) from *E. coli* (PDB code: 1C3O) are shown. In the absence of an available glutamine complex, the structure of the covalent ImGP synthase-acivicin adduct from the *S. cerevisiae* enzyme was used (PDB code: 1OX5). (A) Glutaminase active site of ImGP synthase from *T. maritima*; (B) Glutaminase active site of ImGP synthase from *S. cerevisiae*; (C) Superposition of the glutaminase active sites of ImGP synthase from *T. maritima* and *S. cerevisiae*; (D) Glutaminase active site of CPS. Atom-type colors are used (oxygen, red; nitrogen, blue; carbon, blue, except for ligands (glutamine bound to ImGP synthase from *T. maritima*, green; acivicin bound to ImGP synthase from *S. cerevisiae*, cyan; glutamine bound to CPS, magenta). In panel c, for clarity of superposition, the carbon atoms of ImGP synthase from *S. cerevisiae* are in dark blue. Hydrogen bonds of the reactive side-chain amido group of bound glutamine (ImGP synthase from *T. maritima*, CPS) are shown by dashed lines. The oxyanion hole is properly formed in both glutamine-bound structures, as indicated by the active site-exposed main-chain amido groups of Gly52 (ImGP synthase from *T. maritima*) and Gly241 (CPS), which are marked by asterisks, thus establishing a catalytically competent

conformation of both glutaminase active sites. However, there is no hydrogen bond provided by the oxyanion hole nitrogen atom of Gly51 of ImGP synthase *S. cerevisiae*, which is equivalent to Gly52 of the *T. maritima* enzyme, as there is no functional carbonyl group in acivicin (panels C, D). In a previous study (Chaudhuri et al., 2003), which compared inhibitor-bound structures of ImGP synthase from *S. cerevisiae* and CPS, the preceding residue (Val50) was considered to provide its main-chain amido group for the formation of the oxyanion hole. Some additional key active-site residues are shown and labeled. In the CPS glutaminase active site there is no residue equivalent to Glu96 of ImGP synthase (*T. maritima*). In CPS, the glutaminase active-site cysteine was mutated into a serine (Ser261).

Supplementary Information Available: X-ray data collection and refinement statistics (**Supplementary Table 1**); Schematic view of the reactions catalyzed by HisA and ImGP showing the structures of PrFAR, ProFAR, AICAR and ImGP (**Supplementary Figure S1**); [Stereo version of Figure 2 \(Supplementary Figure S2\)](#); Comparison of relevant structural data from the ImGP synthase from yeast and *T. maritima* (text); Superimposed glutaminase active-site structures (**Supplementary Figure S3**); Reaction conditions for steady state kinetics (methods, text); X-ray structure determination (methods, text); Assays used for steady-state enzyme kinetic analysis (**Supplementary Figure S4**).

Figure 1
[Click here to download high resolution image](#)

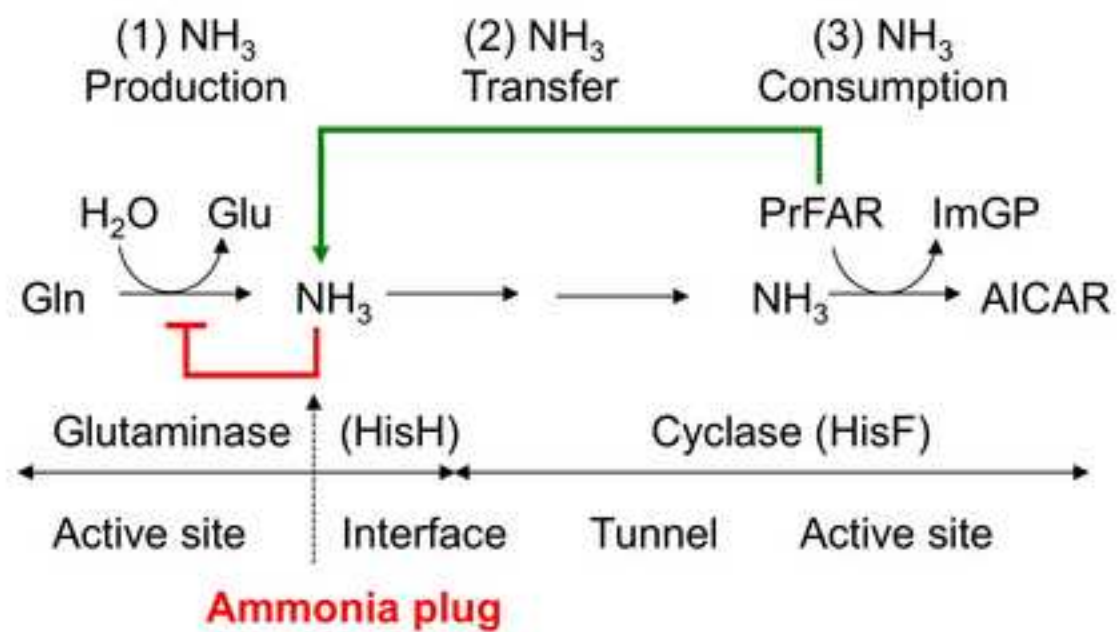


Figure 1

Figure 2
[Click here to download high resolution image](#)

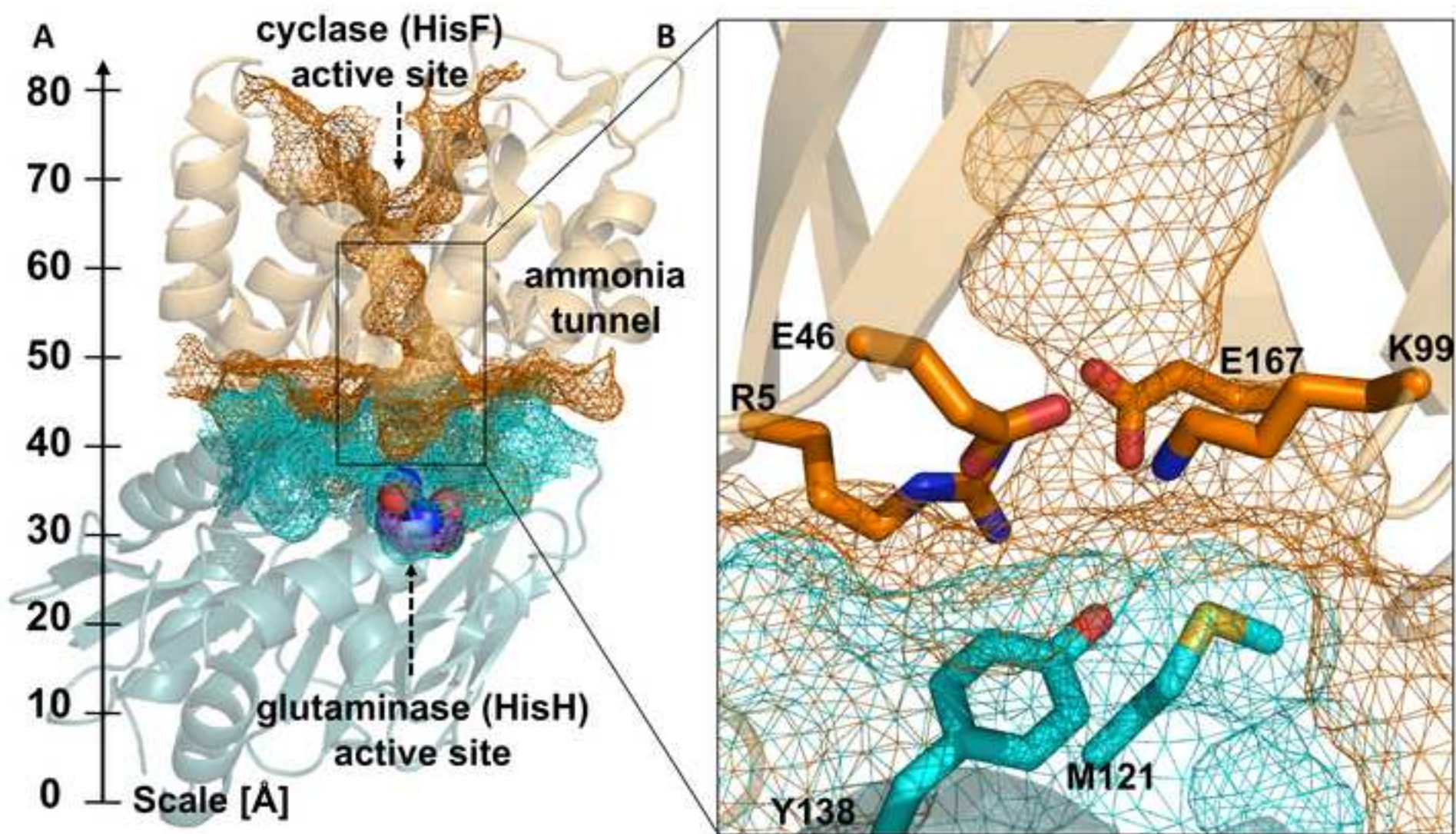


Figure 2

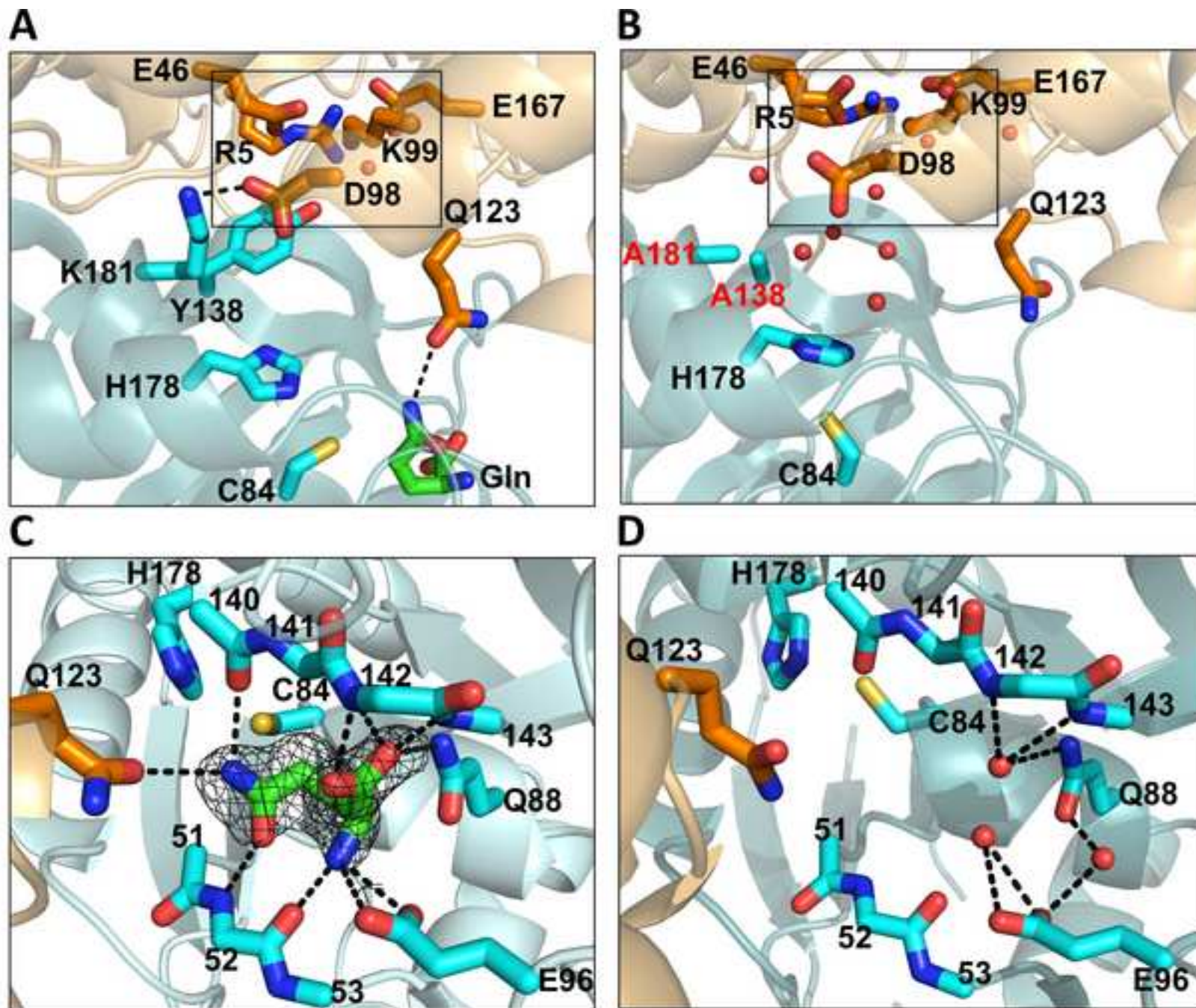


Figure 4
[Click here to download high resolution image](#)

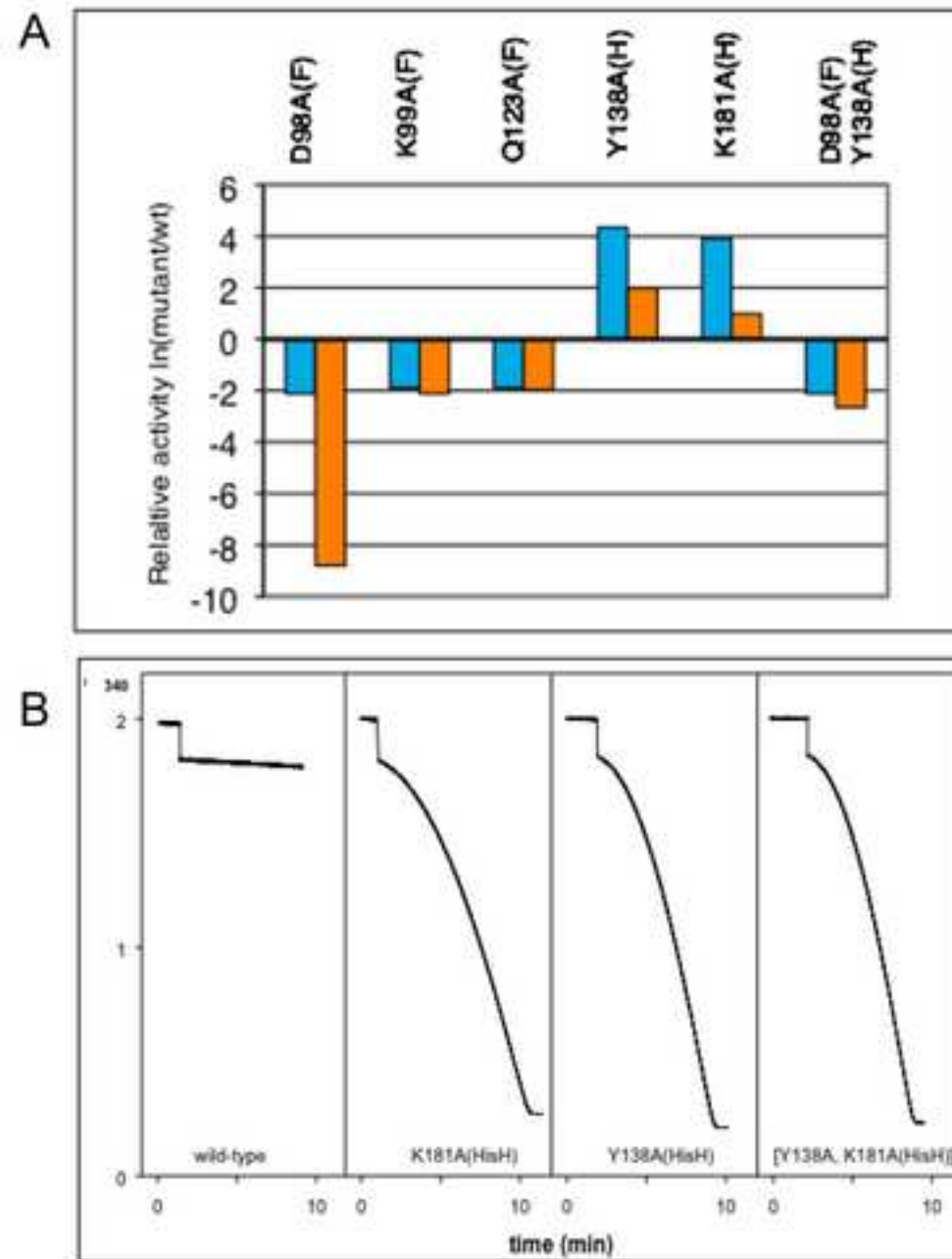


Figure 4

Figure 5
[Click here to download high resolution image](#)

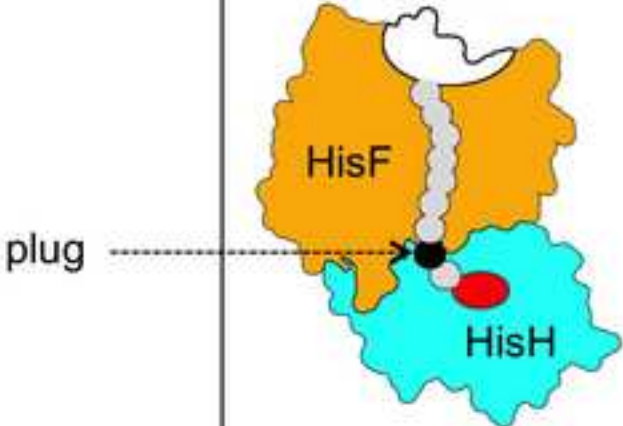

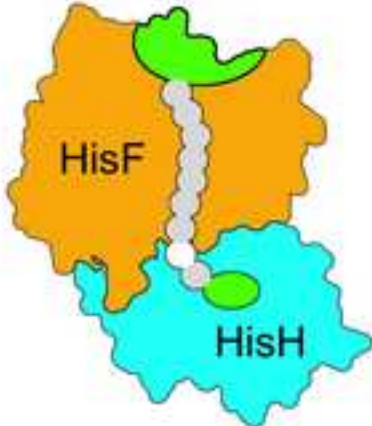
HisF-HisH	A) wild-type	B) Y138A(HisH),K181A(HisH)	C) wild-type
Substrate	Gln	Gln	Gln + PrFAR
			
Glutaminase activity	-	+++	+
Cyclase activity	-	not required	+
Ammonia transfer	blocked	open	open

Figure 5

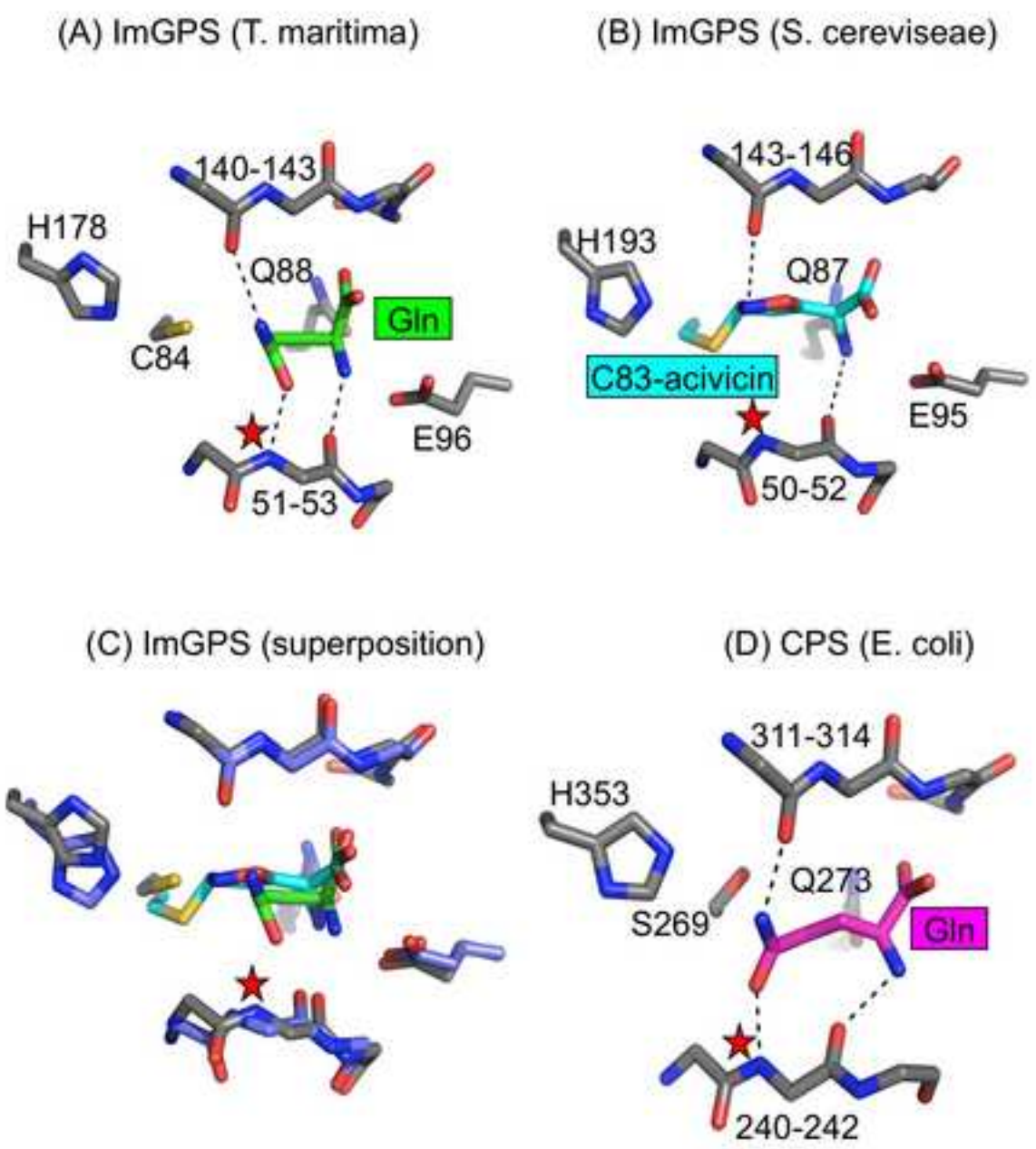


Figure 6

Table 1: Steady-state kinetics of ImGP synthase from *T. maritima*.

Glutamine-dependent cyclase activity (Supplementary Figure S4A)

	K_M^{PrFAR} [mM]	k_{cat} [s ⁻¹]	$k_{\text{cat}}/K_M^{\text{PrFAR}}$ [M ⁻¹ s ⁻¹]	$(k_{\text{cat}}/K_M)_{\text{mutant}} /$ $(k_{\text{cat}}/K_M)_{\text{wt}}$
Wild type	$2,0 \pm 1,2 \times 10^{-3}$	$1,1 \pm 0,1$	$5,5 \pm 0,3 \times 10^5$	1,0
D98A(HisF) ^a	$\gg 5 \times 10^{-2}$	$\ll 4,0 \times 10^{-3}$	8×10^1	$\ll 1,5 \times 10^{-4}$
K99A(HisF)	$1,5 \pm 0,1 \times 10^{-3}$	$1,0 \pm 0,3 \times 10^{-1}$	$6,7 \pm 3,0 \times 10^4$	0,12
Q123A(HisF)	$1,3 \pm 0,4 \times 10^{-3}$	$1,0 \pm 0,2 \times 10^{-1}$	$7,7 \pm 5,0 \times 10^4$	0,14
Y138A(HisH)	$2,0 \pm 0,6 \times 10^{-4}$	$8,0 \pm 0,6 \times 10^{-1}$	$4,0 \pm 0,7 \times 10^6$	7,3
K181A(HisH)	$6,0 \pm 0,6 \times 10^{-4}$	$9,0 \pm 1,0 \times 10^{-1}$	$1,5 \pm 0,3 \times 10^6$	2,7
D98A(HisF), Y138A(HisH)	$2,6 \pm 0,3 \times 10^{-3}$	$1,0 \pm 0,01 \times 10^{-1}$	$3,8 \pm 0,3 \times 10^4$	0,07
Y138A(HisH), K181A(HisH)	not determined	$1,3 \pm 0,1 \times 10^{-1}$	not determined	

Reaction conditions: 50 mM Tris-acetate buffer, pH 8.0, 25 °C, 0.2-2.0 μM HisH or HisH variant, 0.1-1.0 μM HisF or HisF variant, 5-50 mM L-glutamine, 0-40 μM ProFAR.

Ammonia-dependent cyclase activity (Supplementary Figure S4B)

	K_M^{PrFAR} [mM]	k_{cat} [s ⁻¹]	$k_{\text{cat}}/K_M^{\text{PrFAR}}$ [M ⁻¹ s ⁻¹]	$(k_{\text{cat}}/K_M)_{\text{mutant}} /$ $(k_{\text{cat}}/K_M)_{\text{wt}}$
Wild type	$3,6 \pm 0,6 \times 10^{-3}$	$1,2 \pm 0,1$	$3,3 \pm 0,1 \times 10^5$	1
D98A(HisF)	$1,9 \pm 0,7 \times 10^{-3}$	$2,3 \pm 0,1$	$1,2 \pm 0,5 \times 10^6$	3,6
K99A(HisF)	$6,2 \pm 1,8 \times 10^{-3}$	$2,0 \pm 0,2 \times 10^{-1}$	$3,2 \pm 1,1 \times 10^4$	0,10
Q123A(HisF)	$3,3 \pm 1,5 \times 10^{-3}$	$6,0 \pm 1,0 \times 10^{-1}$	$1,8 \pm 0,7 \times 10^5$	0,55
Y138A(HisH)	$1,8 \pm 0,8 \times 10^{-3}$	$1,4 \pm 0,2$	$7,8 \pm 0,4 \times 10^5$	2,4
K181A(HisH)	$9,0 \pm 1,1 \times 10^{-4}$	$1,7 \pm 0,2$	$1,8 \pm 0,4 \times 10^6$	5,5
D98A(HisF), Y138A(HisH)	$2,2 \pm 1,0 \times 10^{-3}$	$2,5 \pm 0,1$	$1,1 \pm 1,0 \times 10^6$	3,3
Y138A(HisH), K181A(HisH)	$2,4 \pm 1,4 \times 10^{-4}$	$8,5 \pm 1,3 \times 10^{-1}$	$3,6 \pm 2,3 \times 10^6$	10,9

Reaction conditions: 50 mM tris-acetate buffer, pH 8.5, 25 °C, 0.2 μM HisH, 0.1 μM HisF, 100 mM NH₄CH₃CO₂ corresponding to 17.4 mM NH₃, 0-40 μM ProFAR.

Glutaminase activity (Glutamate production; Supplementary Figure S4C) (ProFAR added at saturating concentrations)

	K_M^{Gln} [mM]	k_{cat} [s ⁻¹]	k_{cat}/K_M^{Gln} [M ⁻¹ s ⁻¹]	$(k_{cat}/K_M)_{mutant} /$ $(k_{cat}/K_M)_{wt}$
Wild type	8,0 ± 3,0 x 10 ⁻¹	1,0 ± 0,1 x 10 ⁻¹	1,3 ± 0,4 x 10 ²	1
D98A(HisF) ^b			<1,6 ± 0,8 x 10 ¹	< 0,12
K99A(HisF)	1,0 ± 0,2	2,0 ± 0,3 x 10 ⁻²	2,0 ± 0,2 x 10 ¹	0,15
Q123A(HisF)	1,0 ± 0,7	2,0 ± 0,4 x 10 ⁻²	2,0 ± 0,6 x 10 ¹	0,15
Y138A(HisH)	3,0 ± 0,3 x 10 ⁻¹	3,0 ± 0,4	1,0 ± 0,3 x 10 ⁴	77
K181A(HisH)	3,7 ± 0,5 x 10 ⁻¹	2,4 ± 0,2	6,5 ± 0,9 x 10 ³	50
D98A(HisF),Y138A(HisH)	6,0 ± 3,0 x 10 ⁻¹	1,0 ± 0,4 x 10 ⁻²	1,6 ± 0,8 x 10 ¹	0,12
Y138A(HisH),K181A(HisH)	1,6 ± 0,7 x 10 ⁻¹	2,4 ± 0,4	1,5 ± 2,3 x 10 ⁴	115

Reaction conditions: 50 mM tricinehydroxide buffer, pH 8.0, 25 °C, 2-8 μM HisF, 1-4 μM HisH, 40 μM ProFAR, 0-5 mM L-glutamine, 3.8-6.7 mg/ml GDH, 11-20 mM NAD⁺.

Glutaminase activity (Glutamate production; Supplementary Figure S4C) (no ProFAR added)

	k_{cat} [s ⁻¹]	$(k_{cat})_{mutant} /$ $(k_{cat})_{wt}$
Wild type	3,3 ± 1,7 x 10 ⁻⁴	1
Y138A(HisH)	1,5 ± 0,6 x 10 ⁻²	45
K181A(HisH)	2,8 ± 0,5 x 10 ⁻²	86
D98A(HisF),Y138A(HisH)	5,0 ± 3,3 x 10 ⁻⁴	1,5
Y138A(HisH),K181A(HisH)	1,4 ± 0,8	2800

Reaction conditions: 50 mM tricinehydroxide buffer, pH 8.0, 25 °C, 0.15-15 μM HisF, 0.25-10 μM HisH, 10 mM L-glutamine.

Glutaminase activity (Ammonia production; Supplementary Figure S4D) (ProFAR added at saturating concentrations)

	k_{cat} [s ⁻¹]
Wild type	4,4 ± 1,8 x 10 ⁻²
D98A(HisF)	no detectable activity
K99A(HisF)	8,5 ± 2,2 x 10 ⁻³

Q123A(HisF)	$1,1 \pm 0,3 \times 10^{-2}$
Y138A(HisH)	$2,2 \pm 0,3$
K181A(HisH)	$3,3 \pm 0,2$
Y138A(HisH),K181A(HisH)	$1,9 \pm 0,02$

Reaction conditions: 50 mM tricine-hydroxide buffer, pH 8.0, 25 °C, 2 μ M HisF, 1 μ M HisH, 40 μ M ProFAR, 10 mM Gln, 2.1 mg/ml GDH, 10 mM α -ketoglutarate, 300 μ M NADH/H⁺.

^aWithin the tested range of substrate concentration, the initial velocity was a linear function of PrFAR concentration.

^bThe glutaminase activities were too low to be quantified. The catalytic efficiency is therefore below the one determined for the [D98A(F),Y138A(H)] double mutant, which defines the detection limit for the assay.

Supplemental Data

Table S1: X-ray data collection and refinement statistics.

ImGP synthase	wild-type	Y138A/K181A
Ligand observed	Gln	none
Data collection		
Beamline	X13 (DESY)	BM16 (ESRF)
Space group	$P3_2$	$P3_2$
Cell dimensions ($a, c, \text{\AA}$)	85.3, 170.9	93.9, 166.3
Wavelength (\AA)	0.802	0.979
Resolution (\AA) [*]	55.9-2.40 (2.50-2.40)	81.4-2.6 (2.69-2.60)
No. unique reflections	51,685	50,263
R_{sym} ^a	0.052 (0.34)	0.070 (0.42)
$I/s(I)$ ^a	16.8 (2.6)	21.5 (4.4)
Completeness (%) ^b	95.5 (88.9)	99.6 (99.7)
Redundancy ^b	2.4 (2.3)	3.9 (3.9)
Refinement		
Resolution (\AA)	55.9-2.41	39.5-2.60
No. reflections	51,680	50,262
Twin fraction	0.49	0.13
$R_{\text{work}}/R_{\text{free}}$	0.19/0.25	0.18/0.22
No. atoms		
Protein	10,462	10,618
Ligand	20	-
Solvent	204	209
Experimental Wilson B factors (\AA^2)	47.0	65.0
Average atomic B-factors (\AA^2)		
Protein Dimer AB	41.1 [†]	76.6
Protein Dimer CD	42.0	74.2 [†]
Protein Dimer EF	49.4	79.1
Ligand	32.8	-
Solvent	35.8	65.0
R.m.s. deviations		

Bond length (Å)	0.012	0.006
Bond angles (°)	1.457	0.993
Ramachandran statistics		
Favored (%)	1203 (92%)	1227 (94%)
Allowed (%)	93 (7%)	59 (5%)
Outliers (%)	16 (1%)	12 (1%)

^aHighest resolution shell in parentheses

^bImGP synthase bienzyme heterodimer used for structural/functional interpretation.

Supplementary Figures

Figure S1. Schematic view of the reactions catalyzed by HisA and ImGP showing the structures of PrFAR, ProFAR, AICAR and ImGP.

Figure S2. Stereo version of Figure 3, with hydrogen bond distances labeled.

Figure S3: Superimposed glutaminase active-site structures. Apo-ImGP synthase (Douangamath et al., 2002) (carbon atoms, magenta); ImGP synthase-glutamine complex (carbon atoms cyan, this contribution); separate glutaminase subunit of ImGP synthase (Douangamath et al., 2002) (carbon atoms, grey). Atom-specific colors are used for all remaining atoms shown. Bound glutamine is also shown (carbon atoms in green).

Figure S4. Assays used for steady-state enzyme kinetic analysis. (A) Glutamine-dependent cyclase activity; (B) Ammonia-dependent cyclase activity; (C) Glutaminase activity as recorded by glutamate production; (D) Glutaminase activity as recorded by ammonia production. The relations of the assays to the overall reaction scheme of ImGP synthase reaction are also indicated in **Figure 1**.

Supplemental Experimental Procedures

Reaction conditions for steady state kinetics

Glutamine-dependent cyclase assay: 50 mM Tris-acetate buffer, pH 8.0, 0.2-2.0 μM HisH, 0.1-1.0 μM HisF, 5-50 mM L-glutamine, 0-40 μM ProFAR.

Ammonia-dependent cyclase assay: 50 mM tris-acetate buffer, pH 8.5, 0.2 μM HisH, 0.1 μM HisF, 100 mM $\text{NH}_4\text{CH}_3\text{CO}_2$ corresponding to 17.4 mM NH_3 , 0-40 μM ProFAR.

Continuous glutaminase assay to monitor glutamate production: 50 mM tricine-hydroxide buffer, pH 8.0, 2-8 μM HisF, 1-4 μM HisH, 40 μM ProFAR, 0-5 mM L-glutamine, 3.8-6.7 mg/ml GDH, 11-20 mM NAD^+ ; continuous glutaminase assay to monitor ammonia production, 50 mM tricine-hydroxide buffer, pH 8.0, 2 μM HisF, 1 μM HisH, 40 μM ProFAR, 10 mM Gln, 2.1 mg/ml GDH, 10 mM α -ketoglutarate, 300 μM NADH/H^+ . GDH from beef liver was purchased from Roche Diagnostics GmbH (Cat.no. 10197734001). According to the manufacturer's certificate the ammonia concentration was less than 1 μg / mg lyophilisate and the specific activity about 10U / mg lyophilisate. The GDH concentration was adjusted in such a way that further addition of GDH did not accelerate the observed turnover.

Discontinuous glutaminase assay: 0.15-15 μM HisF, 0.25-10 μM HisH, 10 mM L-glutamine.

Glutamate quantification: 100 μ l of the filtrate were incubated with 10 mM NAD⁺ and 0.75 mg/ml GDH for at least one hour at 37 °C in a final volume of 750 μ l.

Glutamate competition assay: ImGP synthase variants were incubated at 25°C with 1.25 μ l [¹⁴C]-glutamine (specific activity 262 mCi/mmol) and 5 mM nonradioactive glutamine in a total volume of 50 μ l of 50 mM tricine-hydroxide buffer, pH 8.0. Samples were prepared in the presence of non-radioactive glutamate at three different concentrations (0, 5 and 20 mM), with/without 40 μ M ProFAR. Reaction conditions, ProFAR present: incubation time 5 min for 1 μ M HisH (all variants except *wt*) and 2 μ M HisF, or 30 μ M *wt* HisH and 60 μ M HisF; reaction conditions, ProFAR absent: incubation time 20 min for 0.6 μ M [Y138A(HisH),K181A(HisH)] and 1.2 μ M HisF, 40 min for 15 μ M Y138A(HisH) or K181A(HisH) and 30 μ M HisF, 4.5 h for *wt* HisH and 90 μ M HisF. A reaction mixture without enzyme was used as a control for spontaneous glutamine hydrolysis. Following incubation, each of the reaction solutions was spun through a 10 kDa filter to remove ImGP synthase. A total of 0.5 μ l of each filtrate was then spotted onto cellulose thin-layer chromatography (TLC) sheets (MN CEL 300-10). The TLC sheets were developed using a solvent system of n-butanol : acetic acid : water (12:3:5, by volume), dried and analyzed by using a phosphor imaging plate (Perkin Elmer). Digital light units were read out with a Cyclone Storage Phosphor System (Packard), using OptiQuant Software. Units, which were generated by [¹⁴C]-glutamate, were normalized with overall units ([¹⁴C]-glutamate and [¹⁴C]-glutamine), within the corresponding lanes after background subtraction. Normalized [¹⁴C]-glutamate units formed in the presence of 5 or 20 mM non-radioactive glutamate are given relative to the

corresponding units of [¹⁴C]-glutamate formed in the absence of non-radioactive glutamate (**Table S1**).

X-ray structure determination

X-ray diffraction datasets were collected at the synchrotron radiation beamlines X13 and BW7B at EMBL/DESY, Hamburg, Germany, and beamline BM16 at the ESRF, Grenoble, at a temperature of 100 K. Intensities were integrated and scaled with MOSFLM (Leslie, 2006) and SCALA (Leslie, 2006), or with HKL2000 (Otwinowski, 1997). Further statistics are summarized in **Table 1**. Submission of the structure factor amplitudes to the Twin server (Yeates and Fam, 1999) revealed that all datasets were pseudo-merohedrally twinned with twin fractions of 0.10-0.49. The three heterodimers of *wt* and [Y138A(HisH), K181A(HisH)] mutant ImGP synthase were positioned and orientated by molecular replacement with AMORE (Navaza, 2001) or with PHASER (McCoy et al., 2007), using the previous apo structure of ImGP synthase (Douangamath et al., 2002) as a search model.

After initial refinement of these coordinates in REFMAC5, phenix.refine (Adams et al., 2004) was used for twin refinement, while retaining non-crystallographic symmetry (NCS) restraints to ensure convergence of refinement at 2.4–2.8 Å. This substantially improved the electron density of the third ImGP synthase hetero-dimer, and the R factor statistics remained within acceptable values. Model building was carried out with TurboFrodo (Roussel et al., 1990) and COOT (Emsley and Cowtan, 2004), and model correctness was assessed with PROCHECK (Laskowski et al., 1993). All cyclase and glutaminase subunits in the asymmetric unit are superimposable with an r.m.s.d. (Ca

atoms) of $0.36 \pm 0.02 \text{ \AA}$ and $0.41 \pm 0.07 \text{ \AA}$, respectively. When the three hetero-dimers are compared, both as rigid and as flexible complexes, the r.m.s.d. is 0.40 \AA (chains AB versus CD) and 0.70 \AA (chains AB or CD versus EF). It is worth noting that the two glutamine complexes (chains AB and CD) are structurally more similar and better ordered crystallographically than the third, glutamine-free hetero-dimer (chains EF). The best defined hetero-dimeric glutaminase/cyclase complex from each crystal form, defined by lowest overall temperature factors and assigned with chains A (cyclase) and B (glutaminase), was used for further interpretation. We have noticed that the final average residual atomic mobility factors in the refined Y138A(HisH), K181A(HisH)] mutant ImGP synthase variant were substantially higher than those of the refined structure of the *wt* bioenzyme (Table S1). We confirmed this difference to be real, as the experimental B_{Wilson} factors were estimated to be 47 \AA^2 for the *wt* bioenzyme and 65 \AA^2 for the Y138A(HisH), K181A(HisH)] mutant.

Supplemental References

Adams, P.D., Gopal, K., Grosse-Kunstleve, R.W., Hung, L.W., Ioerger, T.R., McCoy, A.J., Moriarty, N.W., Pai, R.K., Read, R.J., Romo, T.D., *et al.* (2004). Recent developments in the PHENIX software for automated crystallographic structure determination. *J Synchrotron Radiat* *11*, 53-55.

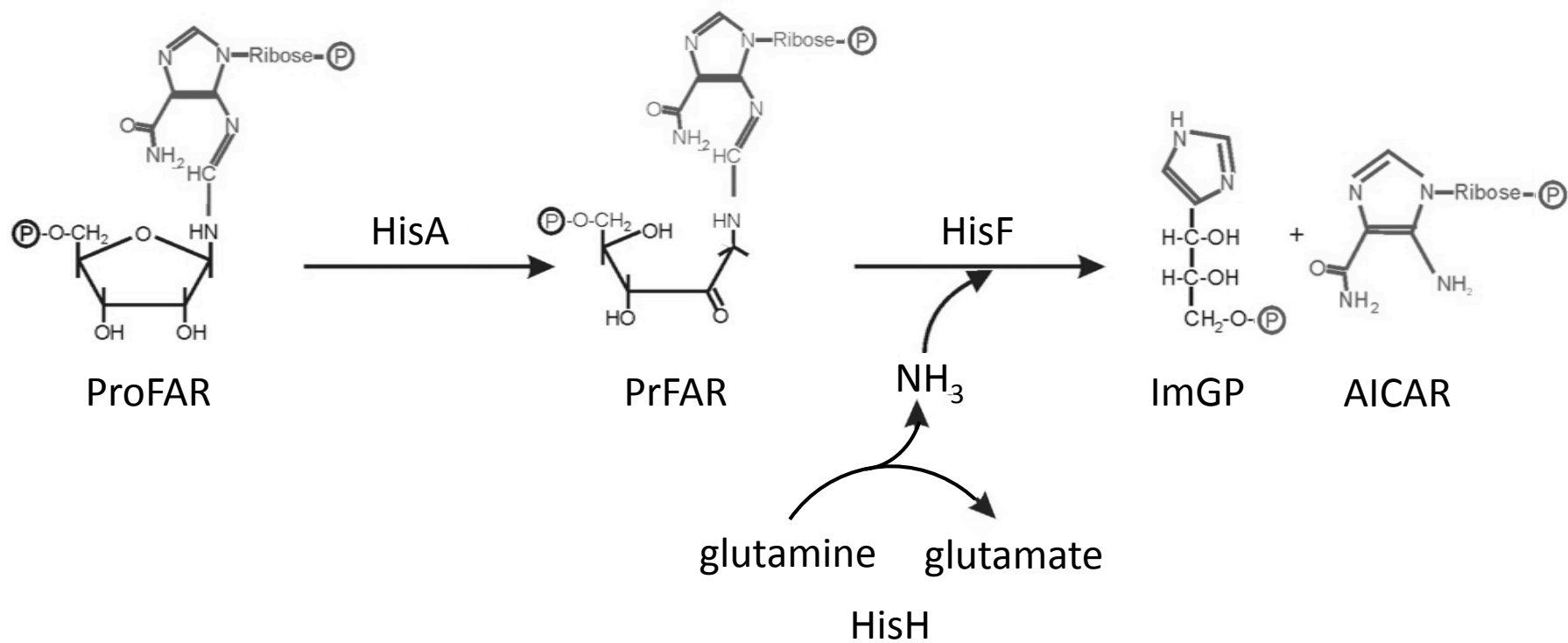
Amaro, R.E., Myers, R.S., Davisson, V.J., and Luthey-Schulten, Z.A. (2005). Structural elements in IGP synthase exclude water to optimize ammonia transfer. *Biophys J* *89*, 475-487.

Chaudhuri, B.N., Lange, S.C., Myers, R.S., Davisson, V.J., and Smith, J.L. (2003). Toward understanding the mechanism of the complex cyclization reaction catalyzed by imidazole glycerolphosphate synthase: crystal structures of a ternary complex and the free enzyme. *Biochemistry* *42*, 7003-7012.

Douangamath, A., Walker, M., Beismann-Driemeyer, S., Vega-Fernandez, M.C., Sterner, R., and Wilmanns, M. (2002). Structural evidence for ammonia tunneling across the (beta alpha)₈ barrel of the imidazole glycerol phosphate synthase bienzyme complex. *Structure* *10*, 185-193.

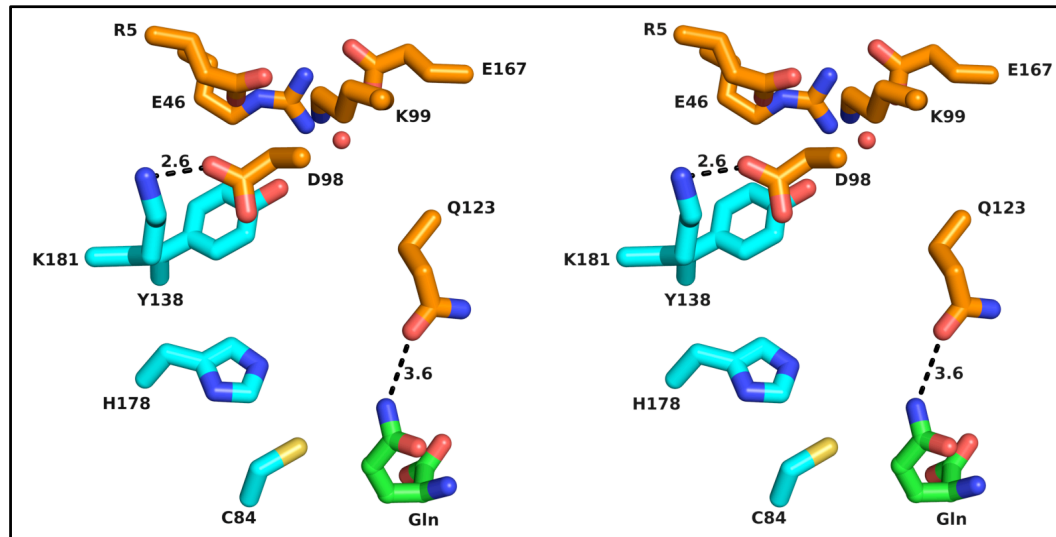
Emsley, P., and Cowtan, K. (2004). Coot: model-building tools for molecular graphics. *Acta Crystallogr D Biol Crystallogr* *60*, 2126-2132.

- Laskowski, R.A., MacArthur, M.W., and Thornton, J.M. (1993). PROCHECK: a program to check the stereochemical quality of protein structures. *J. Appl. Cryst.* *26*, 283-291.
- Leslie, A.G. (2006). The integration of macromolecular diffraction data. *Acta Crystallogr D Biol Crystallogr* *62*, 48-57.
- McCoy, A.J., Grosse-Kunstleve, R.W., Adams, P.D., Winn, M.D., Storoni, L.C., and Read, R.J. (2007). Phaser crystallographic software. *J Appl Crystallogr* *40*, 658-674.
- Myers, R.S., Amaro, R.E., Luthey-Schulten, Z.A., and Davisson, V.J. (2005). Reaction coupling through interdomain contacts in imidazole glycerol phosphate synthase. *Biochemistry* *44*, 11974-11985.
- Navaza, J. (2001). Implementation of molecular replacement in AMoRe. *Acta Crystallogr D Biol Crystallogr* *57*, 1367-1372.
- Otwinowski, Z., Minor, V. (1997). Processing of X-ray diffraction data collected in oscillation mode. *Meth. Enzym.* *276*, 307-326.
- Roussel, A., Fontecilla-Camps, J.C., and Cambillau, C. (1990). CRYStallize: a crystallographic symmetry display and handling subpackage in TOM/FRODO. *J Mol Graph* *8*, 86-88, 91.
- Yeates, T.O., and Fam, B.C. (1999). Protein crystals and their evil twins. *Structure* *7*, R25-29.

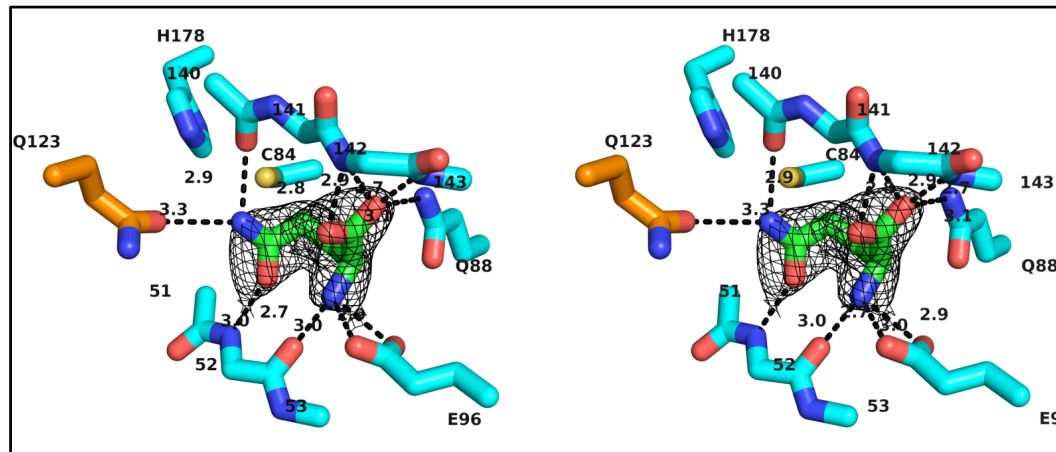


Supplement Figure S1

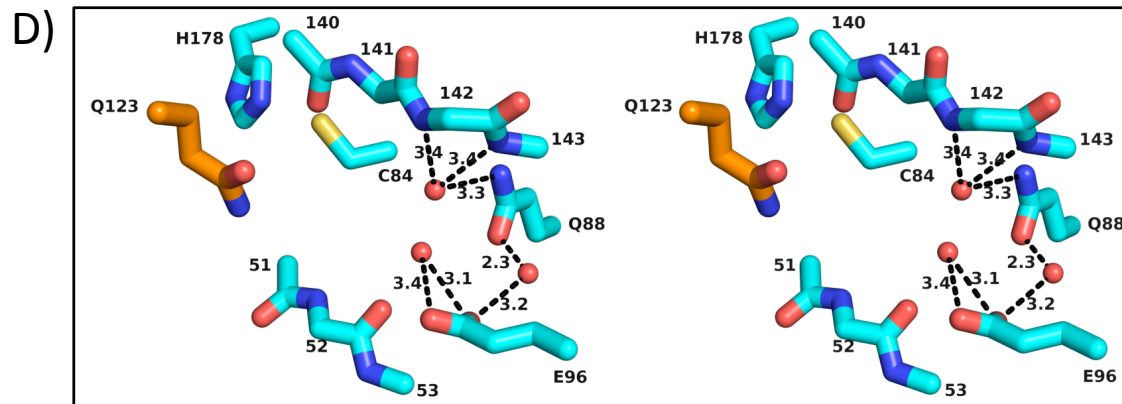
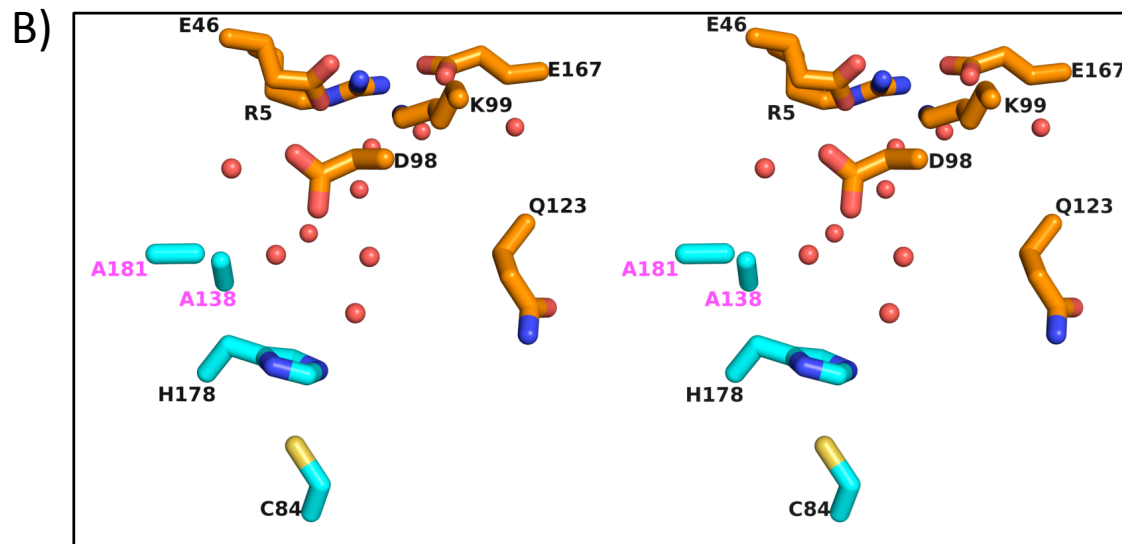
A)



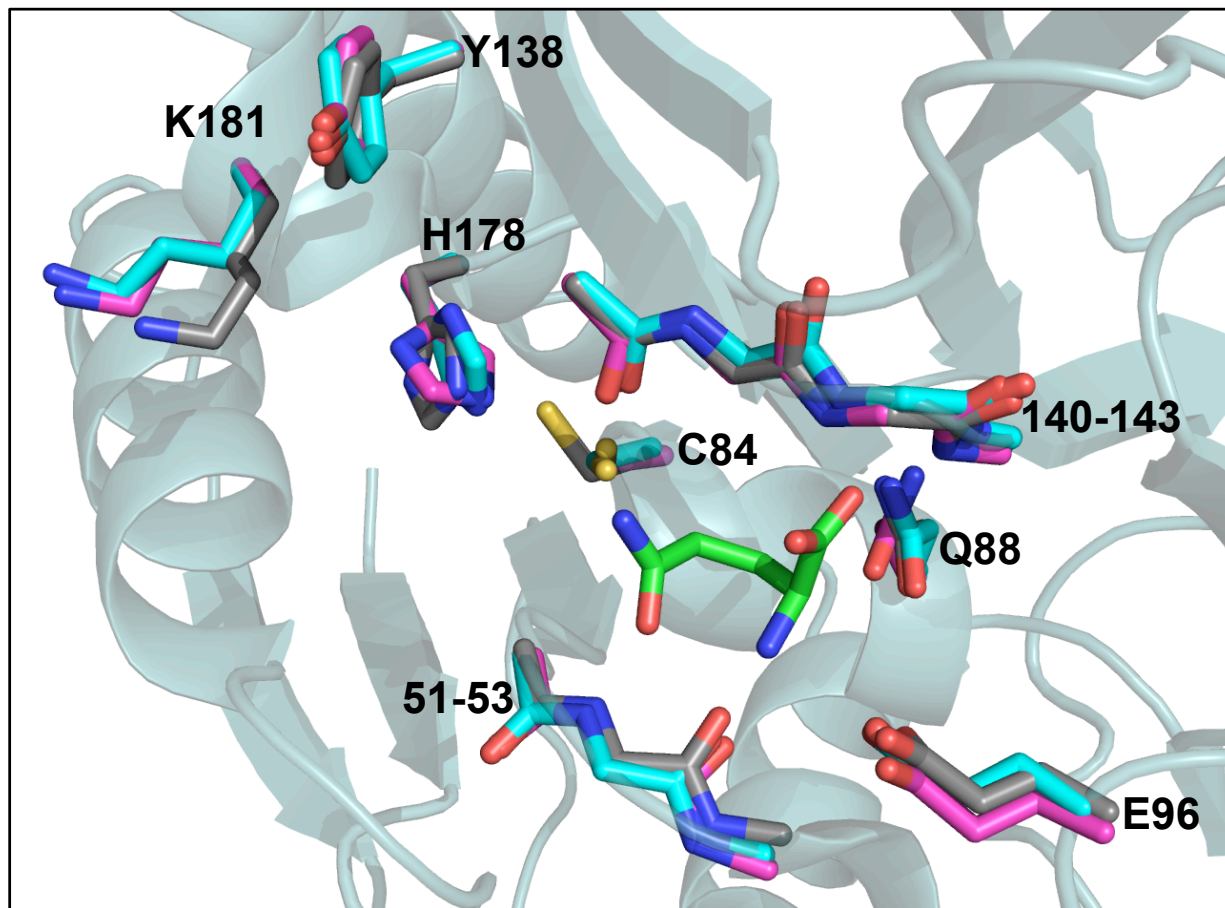
C)



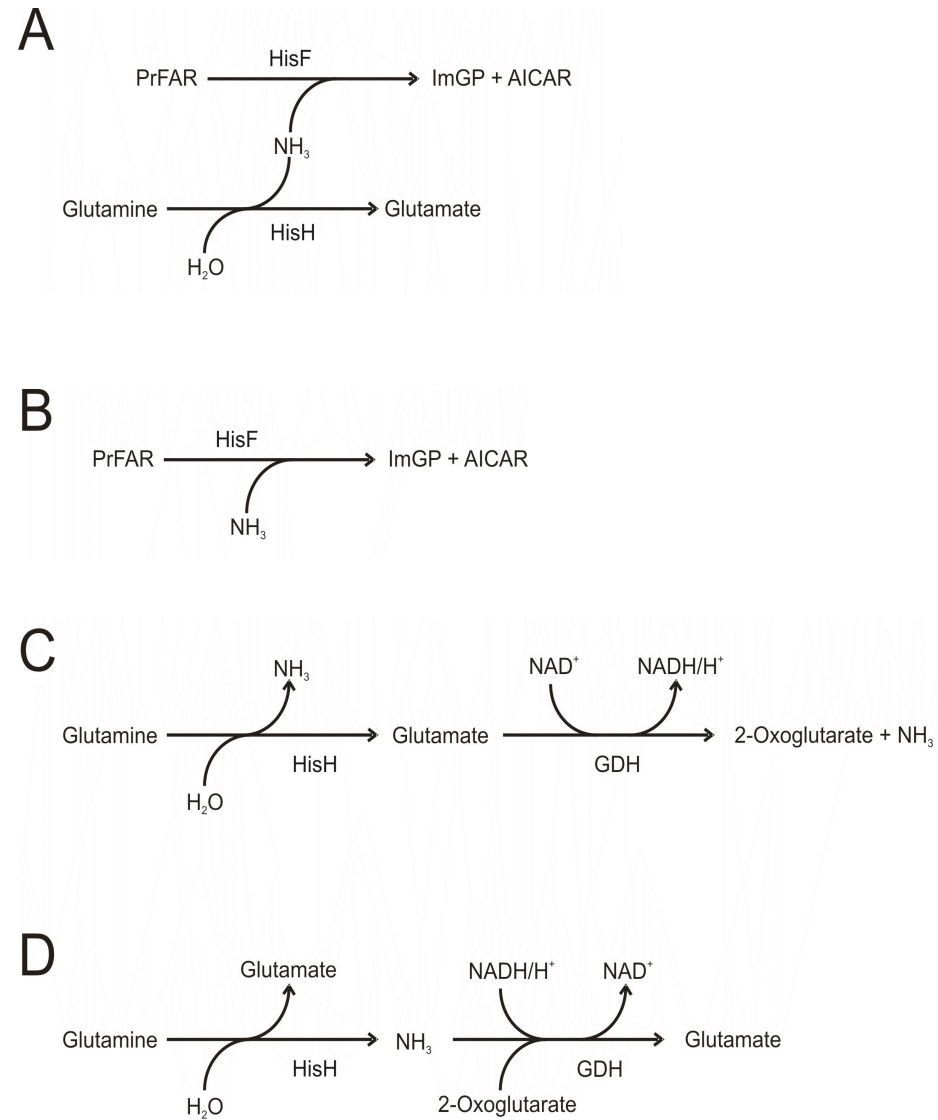
Supplement Figure S2



Supplement Figure S2 (continued)



Supplement Figure S3



Supplement Figure S4